**UNIVERSITATEA BABEȘ-BOLYAI**

**Facultatea de Fizică**

# Teză de licență

**Mihai BĂBUȚAN**

**Conducător științific**

**CS1. dr. Ioan BOTIZ**

**Cluj-Napoca**

**2024**

**UNIVERSITATEA BABEȘ-BOLYAI**

**Facultatea de Fizică**

# TEZA DE LICENȚĂ

---

## Morphological Characteristics of Biopolymer Thin Films Swollen-Rich in Solvent Vapors

---

**Mihai BĂBUȚAN**

**Conducător științific**

**CS1. dr. Ioan BOTIZ**

**Cluj-Napoca**

**2024**

## To my parents

# Acknowledgments

First of all, I would like to show my gratitude to Professor Botiz Ioan, who was my supervising professor for this bachelor's degree. Throughout the time we spent working together, I have come to greatly appreciate his openness to new ideas, his friendly and inclusive character, but above all, his interdisciplinary approach to research and his creative perspective on its place in the world. Thank you for opening my mind and showing me that the boundaries of physics are far more fluid and expansive than they often appeared in most undergraduate courses. I hope working with you again in the near future.

I would also like to express my gratitude to the institute for providing access to high-performance equipment, test substances, and other specialized resources, without which this study would not have been possible.

Also, on a personal level, I would like to thank my parents for supporting me during my bachelor's degree.

Finally, as this work marks the completion of my bachelor's degree, I would like to thank those who have accompanied me throughout these years - Ruxandra and friends professors from the Faculty of Letters. Just as Professor Botiz expanded my perspectives on the scientific world, they dynamited my language, shaking and rebuilding my understanding of the essential role that art, aesthetics, and the artistic spirit play in everyday life.

# Abstract

Biopolymers exhibit a large variety of attractive properties including biocompatibility, flexibility, gelation ability, and low cost. Therefore, especially in more recent years, they have become highly suitable for a wider and wider range of applications stretching across several key sectors such as those related to food packaging, pharmaceutic, and medical industries, just to name a few. Moreover, biopolymers' properties are known to be strongly dependent on the molecular arrangements adopted by such chains at the nanoscale and microscale. Fortunately, these arrangements can be altered and eventually optimized through a plethora of more or less efficient polymer processing methods. Here, we used a space-confined solvent vapor annealing (C-SVA) method to subject various biopolymers to rich swelling in solvent vapors in order to favor their further crystallization or self-assembly, with the final aim of obtaining thin biopolymer films exhibiting more ordered chain conformations. The results obtained by atomic force microscopy revealed that while the gelatin biopolymer nucleated and then crystallized into granular compact structures, other biopolymers preferred to self-assemble into (curved) lamellar rows composed of spherical nanoparticles (glycogen and chitosan) or into more complex helix-resembling morphologies (phytagel). The capability of the C-SVA processing method to favor crystallization and to induce self-assembly in various biopolymeric species or even monomeric units further emphasizes its great potential in the future structuring of a variety of biological (macro)molecules. (this abstract was reproduced from my publication: [1] ).

# Table of Contents

# Introduction

Polymers are the most adaptable class of material and there are constantly shaping our society and life on our planet. These soft molecules are composed of many repeated subunits named monomers, that can be represented in the most varied chemical species, and are linked together in an infinity of models by covalent bonds. [2]

The focus of this study is on biopolymers and poloxamers, which represent a specific category of polymers that carve out a specialized niche in the extensive polymer domain. These materials play a crucial role in the medical sector, primarily due to their remarkable biocompatibility [3], [4], [5] and biomimetic capabilities [6], [7].

Current understanding indicates that the morphology of polymers can be adjusted through a range of processing methods, aimed at optimizing and enhancing their properties through the rigorous control and regulation of molecular arrangements at the macro, micro and nanometric scale. [8]

Our focus on the medical field has highlighted the importance of studying the morphology of films made from chitosan, gelatin, dextrin, phytagel, glycogen, polydopamine, poloxamer 407, and poloxamer 188. Although research on this specific polymeric films is sparse, it is vital for advancing our knowledge and utilization of these biopolymers and poloxamers in creating enhanced biomedical materials. Comprehensive information and references regarding their monomeric structure and utility are available in Chapter 1, particularly in subsections 1.1 and 1.2.

Among the various techniques documented in the literature for the production of these films—such as spin casting, drop casting, dip coating, and spray coating—we opted for the spin casting method to achieve high-quality biopolymeric and

poloxamer-based films. This approach utilizes the rapid dispersion of a polymer solution onto different solid substrates, facilitated by centrifugal forces generated through spinning. A significant benefit of this method is that the liquid film tends to attain a uniform thickness during the evaporation phase if the liquid film consists of a nonvolatile solute and a volatile solvent [9]. In terms of processing, we utilized the solvent vapor annealing in a quasi-confined environment (C-SVA) method, which have been described in detail in subsection 1.3. The specific details of our film fabrication and processing methodology are discussed in Chapter 2.

Following processing, both the processed and unprocessed films were examined using optical microscopy and AFM measurements. This analysis highlighted the impact of spin casting and the C SVA method on the morphology of biopolymeric and poloxamer-based solutions. A comprehensive discussion on the resulting films and the phenomena they underwent, including various types of self-assembly, is presented in Chapter 3 for the biopolymeric samples and in Chapter 4 for the poloxamer-based probes.

# Chapter 1

# Biopolymers and Poloxamers as fundamental materials for medical and industrial applications

## 1.1 Aminoacid-based and glucose-based biopolymers

In recent years, there is an increasing demand for biodegradable materials manufactured using biopolymers [10], [11], [12], [13], due to growing concerns about product sustainability issues. It is a more feasible choice due to the fact that biopolymers are readily available, being produced by living organisms in the form of saccharides (such as chitosan, dextrin, glycogen, or phytagel)[14], [15], [16], proteins (like gelatin, collagen, or fibroin)[17], [18], [19], [20], or DNA[21], [22].

Aminoacid-based biopolymers have 4 specific structural levels – primary, secondary, tertiary, respectively quaternary structure – each possessing unique physical properties that contribute to the overall properties of the resulting biopolymer [23]. Because of this structural variety, which is a characteristic of proteins, the environment in which an amino acid chain is created or its place of origin can have an impact on its set of macroscopic features. As a result, protein biopolymers can perform a wide range of specialized functions, when are processed differently and adopting specific molecular arrangements. For example, gelatin is used in the design and development of medical applications, such as drug delivery [24], [25], [26], wound dressing and tissue healing hydrogels[27], [28], [29], or as an additive for contrast enhancement [30]. When

deposited on solid surfaces, gelatin can exhibit characteristic coiled-like conformations, such as a nanoparticle structure [31].

Polysaccharides consist of extensive chains of monosaccharides linked together by glycosidic bonds, which are typically utilized by our bodies for energy production or to support cellular structure. Moreover, because of their strength, steadiness, flexibility, and biocompatibility, glucose-based biopolymers have a high utility value in the food industry [32], [33], in medical applications such as drug delivery [34], [35], [36], [37], hydrogel and scaffold production for cell growth and tissue engineering [38], [39], [40], in the construction of various functional biomaterials [36], [41], as therapeutic and contrast agents [42], or in other fields of application [43], [44], etc. For instance, chitosan, a widely recognized biopolymer, typically forms fibrillar or porous structures when casted to solid surfaces, and is utilized in drug delivery systems as well as in anti-microbial applications [45], [46]. Dextrin and glycogen, although sharing the same monomer (glucose), serve distinct purposes across multiple industries, such as food packaging and electronics [47], [48]. Other notable biopolymer is phytagel as a saccharide that plays multiple roles in the fabrication of hydrogels and scaffolds [37], [49], [50].

Polydopamine is a biopolymer exhibiting novel functions because of its chemical structure comprised of a catechol fraction and an amine side. Considering its functional groups, polydopamine has an important role in the construction of multifunctional hydrogels (including modified hydrogels for medical treatments), where it can be integrated as a stabilizer in the hydrogel network via three different structures including chains, coatings, and nanoparticles [51], [52]. Obviously, polydopamine is composed of dopamine monomer units. The latter can assemble into highly ordered structures which can subsequently be utilized in combination with other (bio)polymers. This approach is particularly promising for the development of innovative composite materials

for spinal cord injuries, bio-adhesives as well as for applications in biomimetics and antibacterial solutions [53], [54], [55], [56], among others.

## 1.2 Poloxamers and functional materials

Poloxamers, also known as Pluronic systems, are a category of water-soluble nonionic triblock copolymers characterized by their A-B-A and B-A-B structures, with A being poly(ethylene oxide) (PEO) and B representing poly(propylene oxide) (PPO) [57], [58]. Due to their amphiphilic characteristics in water, poloxamers self-assemble into micelles, with the hydrophobic sections forming the inner core and the hydrophilic portions creating the outer surface [59], [60]. Hydrogels, which are created through the micellar property of various Pluronic-based systems, are enhanced with additional substances and biopolymers to develop functional biomaterials. These materials are utilized in numerous areas, particularly in medicine for applications like drug delivery [61], [62], [63], wound dressing and healing [64], [65], tissue engineering [66], [67], and bone repair [68], among others [55]. Specifically, poloxamer 407 or differently marketed as Pluronic F127, is one of the most widely utilized triblock copolymers in medicine, particularly as a hydrogel combined with other biopolymers and nanoparticles for drug delivery [69], [70, p. 407], [71]. Its popularity stems from its biocompatibility, thermosensitive characteristics, and antimicrobial properties. With a lower molecular mass than P407, Poloxamer 188 is another polymer with potential uses in biomedical science and applications. It has unique properties that make it useful for applications in areas such as drug delivery [72], [73], [74] and tissue engineering[66], [75], [76], among others[77], [78], [79].

## 1.3. Theoretical perspective and experimental approach

The property of all these biopolymers is largely dependent on the final (film) microstructure and, consequently, on the molecular configurations that biopolymer chains adopt the nanoscale or microscale level. Thus, to optimize the use of (bio)polymers in any kind of application, it is necessary to take advantage of the relationship between structure, processing, and property (and, eventually, manipulate and comprehend their ordering into different micro-/nanostructures) as well as the correlation between these resulting structures and their macroscopic properties. Therefore, in order to produce a particular desirable microstructure, one must always identify the best processing procedure, usually for each biopolymer system. Fortunately, a wide range of more or less effective processing methods are now available and have been documented in the literature. The majority of these methods rely on basic physical processes like self-assembly [47, 48] and crystallization [49]; these two processes have recently been used to create a variety of functional biomaterials and gels that show great promise for the treatment of wounds and diseases [50–53]. Such (bio)polymer processing techniques, for instance, can rely on hot pressing, solvent vapor annealing, thermal and melt annealing, or the use of space confinements.

Here, we suggest modifying or enhancing the microstructure of films composed of various biopolymeric systems through a processing technique known as solvent vapor annealing in a quasi-confined environment (C-SVA). This approach is designed to promote and/or facilitate self-assembly and crystallization processes, being recently verified on several polymer systems, including diverse diblock and triblock copolymers [80]. It is based on the concept of the rich swelling of (bio)polymer thin films in solvent vapors [81], [82].

The utilized C-SVA equipment consists of a shallow aluminum sample chamber that is sealed with a glass cover and connected to a source of solvent vapors. The bottom of the chamber is placed on a temperature control mechanism composed of a Peltier element, a state-of-the-art temperature controller, and a temperature

sensor so that the temperature of the sample sitting on the bottom of the chamber can be maintained at a specific setpoint within a variation of only 0.01 ◦C for as long as it is needed. Generally, thin films of a specific biopolymer are inserted into the sample chamber, which is then filled with solvent vapors. Furthermore, by lowering the sample temperature, the solvent vapors are forced to condense onto the film sample. As a consequence, the film undergoes rich swelling until it transforms into a "quasi-two-dimensional (2D) film solution". Later on, by reversing the current direction in the Peltier element, the sample temperature can increase as slowly as 0.01 ◦C/s, allowing the solvent molecules to evaporate at a really low rate and thus favoring the films to self-assemble and/or crystallize into (highly) ordered structures.

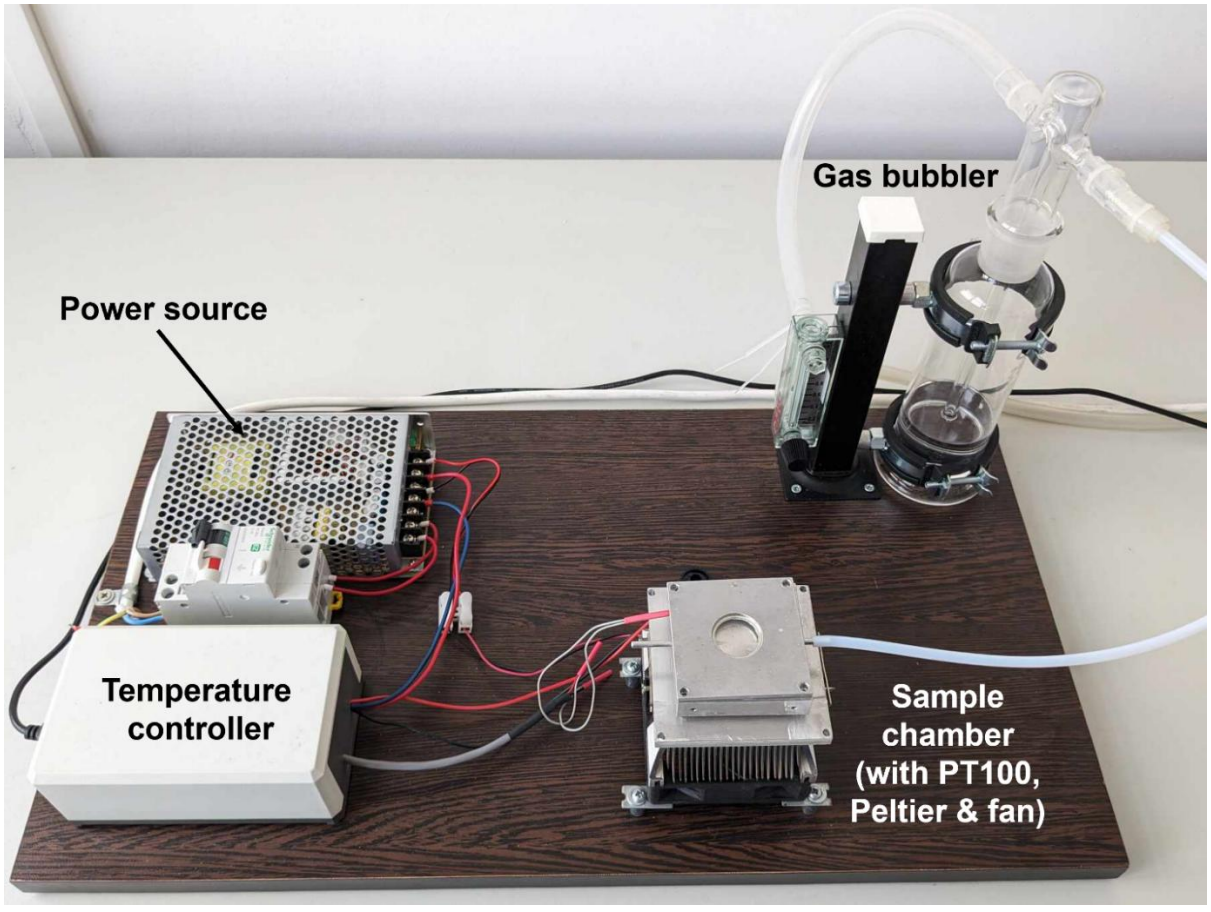


Figure 1. Digital photograph of the home-made C-SVA experimental setup used in this work and comprised of an aluminum sample chamber (equipped with a PT100 temperature sensor, a Peltier

element and a heat evacuating fan), a temperature controller, a power source and a gas (e.g. nitrogen) bubbling system (capable to introduce a controlled amount of solvent vapors into the sample chamber). Image reproduced with permission from ref. [1].

NOTE: Parts of the text from this theoretical chapter were utilized/adapted from the article that was previously published by us: [1]

# Chapter 2

# Materials and Methods

## 2.1 Researched materials

### 2.1.1 Water soluble biopolymers

All polymers used in this work were purchased from sigma alderich. . Dextrin (product number 31400) is a sweet sugar extracted from potato starch and has the linear formula $(C_6H_{12}O_6)_x$. A solution of dextrin was prepared by stirring, at room temperature, 1.5 g of dextrin powder in 30 mL of ultrapure water (solubility 0.5 g in 10 mL of hot water; the white- to faint yellow-colored powder leads to an almost colorless solution at the solubility limit). Glycogen is a branched glucose polymer synthesized by animal cells for energy storage and release. In this instance (specifically product number G8751), the glycogen was extracted from oysters. To prepare a solution, 6.75 g of this glycogen was dissolved in 50 mL of ultrapure water. For phytagel (also known as gellan gum, product number P8169; molecular weight 1000 kg/mol; solubility 10 mg in 1 mL of hot water; white- to off-white-colored powder leads to a colorless to faint yellow solution at the solubility limit) the ultra-pure hot water was used to form a solution with the concentration of 10 mg/ml. Furthermore, solutions of gelatin (product number G9391; solubility 50 mg in 1 mL of water; at the solubility limit, gelatin solution exhibits a faint yellow to yellow or brown-yellow color) and dopamine hydrochloride (product number H8502; molecular weight 189.64 g/mol; solubility 100 mg in 1 mL of water; the white to yellow with a tan cast-colored powder leads to a colorless to dark yellow and colorless to light brown and yellow-brown solution at the solubility limit) were also prepared using

ultrapure water, with the resulting concentrations of 10 mg/mL, respectively 20 mg/mL.

### 2.1.2 Acetic acid soluble biopolymers

Water was substituted for acetic acid as a solvent and a 10 mg/mL solution of chitosan of medium molecular weight (with a range of 190–310 kDa, product number 448877) was prepared.

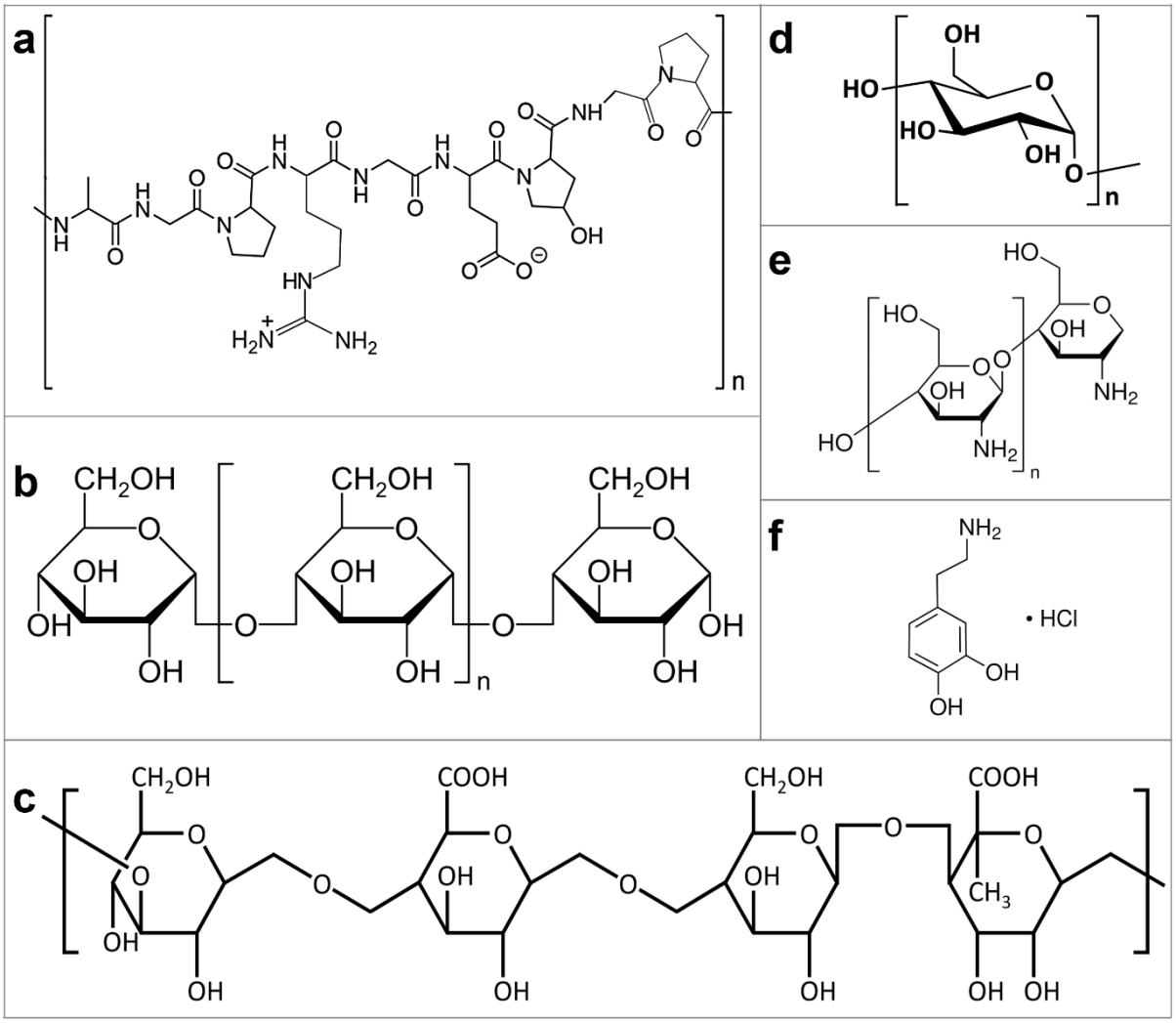


Figure 2. Chemical structures of different biological systems that have been used in this work: gelatin (a), dextrin (b), phytagel (c), glycogen (d), chitosan (e), and dopamine hydrochloride (f). Image reproduced with permission from ref. [1].

### 2.1.3 Poloxamers

For a solution of Poloxamer 188, a quantity of 1 g of P188 powder (product number P4894, water soluble 100 mg/mL, clear, colorless to almost colorless) was mixed with 50 ml of ultra-pure water to obtain a concentration of 20 mg/mL. Finally, with a concentration of 20 mg/mL, one more solutions was obtained using the same solvent and adding F127 powder (product number P2443, molecular mass of 12600 g/mol and solubility ) also known as Poloxamer 407. In order to favor the complete dissolution of the (bio)polymers in the chosen solvent, often, the resulting polymeric solutions were additionally subjected to annealing at a temperature of about 70 °C in a silicon oil bath (ONE 7-45, Schwabach, Germany) for 30 min, followed by filtering with 0.22 μm or 0.45 μm polyvinylidene fluoride/polytetrafluoroethylene microfilters from Millipore.

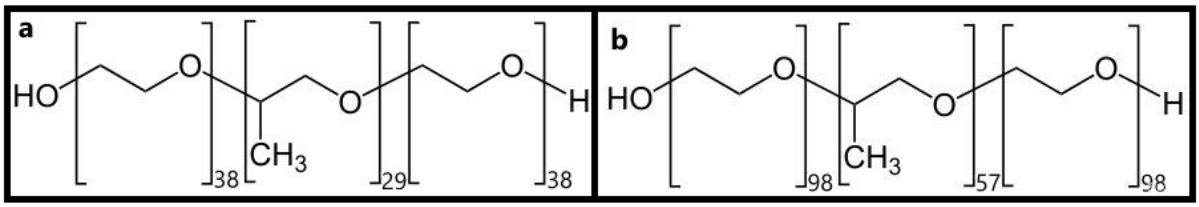


Figure 3. The chemical structures of the polymeric systems examined in this work: a)Poloxamer 188; b)Poloxamer 407.

### 2.1.4 Solid substrates and their cleaning

Silicon wafers (type 4P0/5–10/380 ± 15/SSP/TTV < 5 from Siegert Wafer (Aachen, Germany)) were used as surface for all fabricated thin films. These substrates were cleaned in UV-ozone for 20 minutes, prior to any further use.

## 2.2 Material processing methods

### 2.2.1 Spin casting thin films of (bio)polymers

Samples from each polymer solution were dropped separately onto silicon wafers and and further spincast at 2000 rpm for 30 seconds using a WS-650mz23nppb spin coater from Laurell Technologies Corporation (North Wales, PA, USA). This procedure resulted in the formation of homogeneous biopolymeric films with the following thicknesses: approximately 116 ± 8 nm for glycogen, 111 ± 7 nm for dextrin, 93 ± 5 nm for phytagel, 89 ± 5 nm for gelatin, 97 ± 6 nm for dopamine, and 86 ± 5 nm for chitosan. The thickness of each film was measured by analyzing the cross-sectional profile of a scratch using the atomic force microscopy (AFM) technique. Note that the use of unfiltered solutions in the initial spin casting series resulted in films exhibiting numerous large and dense aggregates dispersed across the entire surface. These films of bad quality indicated that water was not an ideal solvent for such biopolymers (neither was the acetic acid for chitosan). Following the filtration of undissolved biopolymeric aggregates from the solutions, highly homogeneous and uniform thin films were obtained. The main characteristics of the biopolymer systems used and their corresponding spin-cast films are summarized in Table 1.

### 2.2.2 Processing of biopolymer thin films via C-SVA method

Thin biopolymer films underwent a swelling process rich in solvent vapors due to the condensation phenomenon, followed by gradual evaporation of these vapors. This entire process was conducted in a custom-built experimental setup, which included an aluminum sample chamber with a depth of less than one millimeter and a high-performance Peltier element (15.4 V/8.5A from Stonecold) positioned beneath it. The precise regulation of the probe's temperature was achieved through an advanced temperature controller (TCM U 10A from Electron Dynamics Ltd., Southampton, UK), which received feedback from a PT100

temperature sensor situated in the chamber near the sample (detailed descriptions of the experimental setup can be found in references [62,63]). Initially, a nitrogen bubbling system was employed to generate and regulate the amount of solvent vapors accurately within the sample chamber, while maintaining the film sample at an elevated temperature of 40°C. Subsequently, the sample temperature was gradually reduced at a rate of 0.3°C/s to a range of 18-22°C. It is important to note that the exact temperature depended significantly on the type of solvent used, its volatility, and the specific biopolymers being processed. This temperature reduction induced the condensation of solvent vapors onto the film sample. The condensation of solvent vapors was invariably accompanied by a noticeable change in the interference colors. These changes were visible under an optical microscope or to the naked eye, particularly when non-transparent substrates such as silicon wafers were used. This color change was attributed to the significant increase in the film's thickness (further details on this phenomenon and the methods for evaluating film thickness during swelling and deswelling are available in references [58,61]). Upon reaching a state where the film was swollen with condensed solvent vapors, it effectively became a quasi-2D "solution." At this stage, the film sample was subjected to a slow heating process at a controlled rate of 0.01°C/s, gradually bringing the temperature back up to 40°C. This controlled heating triggered a very slow and regulated evaporation of the solvent, thereby promoting processes such as self-assembly or crystallization. Through this method, the biomolecules within the film were able to achieve an orderly and structured arrangement. Once all solvent molecules were completely evaporated from the biopolymer film, the newly dried films displayed the same thickness as they had prior to the swelling process. However, the microstructure of these films was significantly altered and modified, we do not expect that it induced chemical alterations of our biopolymers (except for the case of dopamine hydrochloride, which is expected

to polymerize upon spin-casting and further C-SVA processing into polydopamine).

## 2.3 Material investigation methods

### 2.3.1 Optical microscopy

In order to acquire an overall perspective on the formed systems (order of size 200-300 μm), later being able to choose the areas of interest for the detailed study through the AFM technique, we used a KERN OKN-177 Optical Microscope Kern Sohn Gmbh Balingen, Germany) working in the reflectivity mode and equipped with various magnification objectives, along with KERN ODC 825 (5 Mp) camera (connected to a computer via Microscope VIS software).

### 2.3.2 Atomic force microscopy

The Atomic Force microscope has three main components responsible for the fundamental principle of the AFM technique. The first component is the tip that interacts with the observed probe, raster scanning it in different modes of operation (the two well defined groups of operating modes are contact mode and tapping mode). The tip is attached to a small cantilever that forms a spring and bends as the first component contacts the surface. This bending is indicative of the tip-sample interaction force and is it detected with the third assembly of components consisting of a laser diode and a split photodetector.

In contact mode, the tip is pressed into the surface and an electronic feedback loop monitors the tip-sample interaction force to keep the deflection constant throughout raster scanning. In tapping mode, the cantilever is caused to vibrate near its resonance frequency. The contact of the tip with the probe is

minimal as the tip subsequently moves up and down in what is described as a sinusoidal motion. A feedback loop is used to keep the amplitude of this tapping motion constant as the movement of the tip is modified by the attractive and repulsive interactions with the probe. By this method, the topography of the sample is traced line by line, protecting both the sample surface and the tip from damage.

In this case, AFM measurements were conducted using a system from Molecular Devices and Tools for Nano Technology (NT-MDT) fixed on an Olympus IX71 optical microscope operating in non-contact (tapping) mode. The whole AFM system was acquired from Spectrum Instruments Ltd. (Limerick, Ireland). High-resolution Noncontact Golden Silicon probes from NT-MDT, with a tip radius smaller than 10 nm and a tip height ranging between 14 and 16 μm, were used to visualize the biopolymeric surfaces. These probes were coated with gold on the cantilever's detector side and displayed a length of 125 ± 5 μm and a resonance frequency of 187–230 kHz. They further exhibited a nominal force constant between 1.45 and 15.1 N/m. Moreover, for softer samples, NANOSENSOR PPPNCSTR probes with tip radius smaller than 7 nm were employed, featuring dimensions of 150/27/2.8 μm (length/width/thickness), a force constant of 7.4 N, and a resonance frequency of 75 kHz to 265 kHz. AFM images were captured at a 256 × 256 line configuration, with a scanning speed between 1 and 2 μm/s and a setpoint voltage of 9-12 V, adjusted to maintain a constantly soft tapping regime.

NOTE: Parts of the text from this theoretical chapter were utilized/adapted from the article that was previously published by us: [1]

# Chapter 3

# Growth of diverse nano-shapes of biopolymers through self-assembling and crystallization processes

## 3.1 Short summary

The self-assembling process represents the spontaneous organization of individuals molecules through non-covalent interactions and under thermodynamic conditions into more complex and stable polymeric systems[83].

Crystallization process, encountered in this study, is a type of self-assembling that is commonly utilized to form orderly patterned aggregates, sometimes with peculiar periodicity. Although, there are plentiful studies on the subject of self-assembly bio-polymers [84], [85], [86], this work is qualitative complementary for the field. Similar information about the resulted morphologies in our studies have not been published in other papers.

In this chapter, there are presented the AFM images that describe the nano-scaled architecture of gelatin, dextrin, phytagel, glycogen, chitosan, and dopamine hydrochloride before and after self-assembling process. Each image is followed by our scientifical interpretation of the specific illustration.

### 3.2 Gelatin's granular structure

We start our discussion by presenting the case of gelatin biopolymer. In a general investigation of the AFM images displayed in Figure 3 a,c , it is observed that exposing a thin film of gelatin to ultrapure water vapors via C-SVA technique led to the formation of granular-like structure of elongated shapes. Randomly, yet homogeneously, distributed over the whole film surface, with their margins reminding of fractals, these structures exhibited a length of about 695 ± 80 nanometers and a width of about 375 ± 75 nm. While these structures are too small to be observed forming in detail in the swollen film solutions under the optical microscope, very weak macroscopic changes in the surface homogeneity can be observed for very short times. Such changes usually point toward the material's structuring [81] but with no possibility of seeing the growth in real time. As a consequence, we suggest that the here-presented gelatin structures nucleated and grew during the C-SVA processing and thus, most probably, exhibit a crystalline nature. Interestingly, the AFM height images further accentuated that all gelatin structures displayed a three-dimensional shape, each made up of two fractal-like structures layered on top of each other. The upper structure had an average height of approximately 16 ± 2 nm. Although it is rare for bio-polymer structures to grow in the third direction, they have been observed to form in thin films of polypeptides that were also swollen-rich in solvent vapors[81], [82]. The gelatin structures also contained spherical components with an average size of about 38 ± 6 nm (Figure 3g). Conversely, the space between the 3D granular structures was occupied by much smaller structures, each with an average width of about 14 ± 3 nm (Figure 3h). These latter conformations were similar to those covering the surface of the reference gelatin films that were obtained by spin casting but were not further exposed to water vapors via C-SVA (Figure 3f,i). In these unexposed films, the

surface was smooth, showing no granular structures (Figure 3b,d). In the existing research, a variety of surface morphologies for gelatin have been described, including smooth and densely packed surfaces [87], [88], as well as rough textures [89], often protrusion and/or aggregate-like structures [90]; from sponge or coral-like features [91] to nanoparticles [92]; and from irregular cavities with interconnections [93] to other (fiberbased) networks [94], to the best of our knowledge, no data has been discovered to support the presence of granular 3D crystalline structures, as detailed in this study.

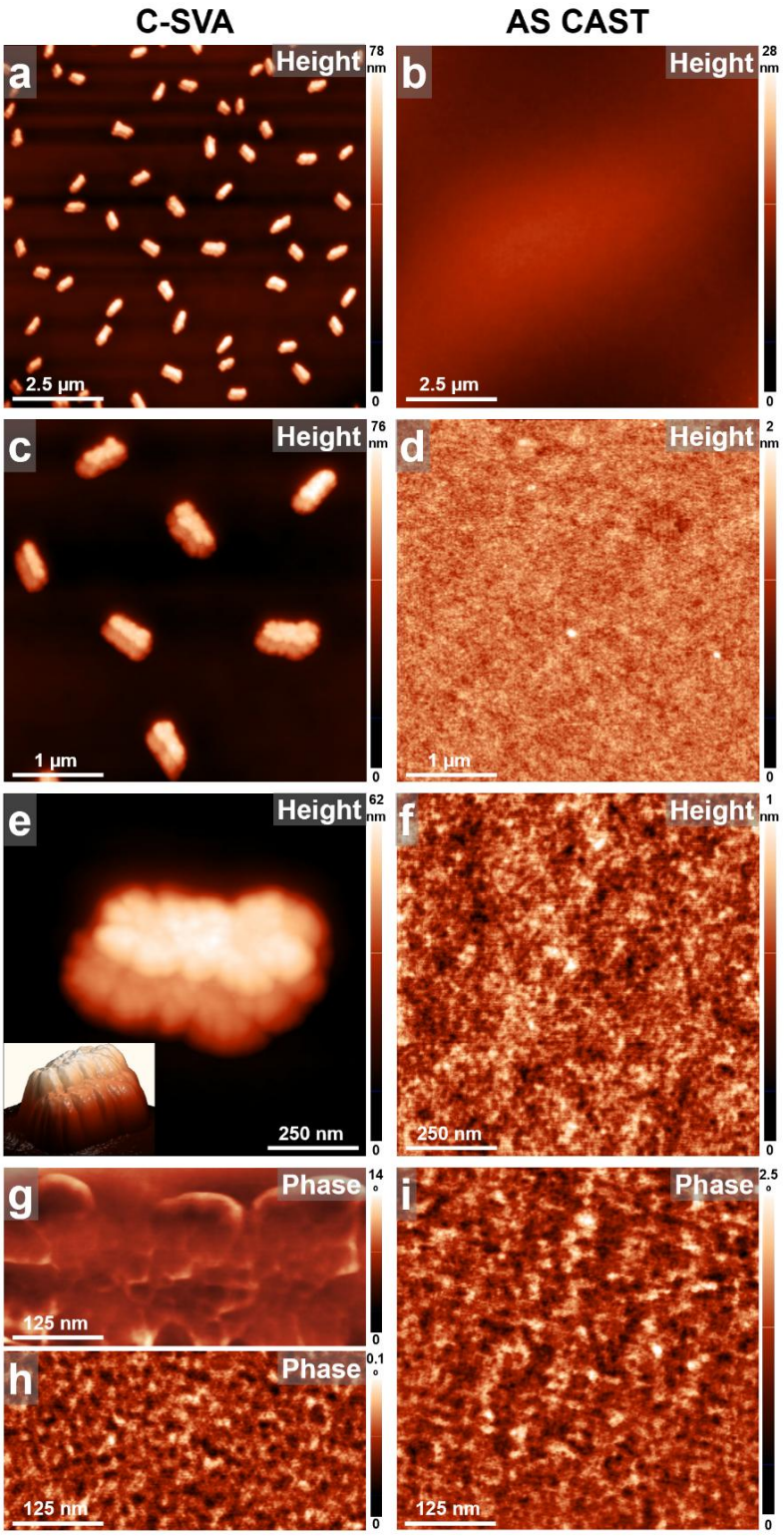


**Figure 4.** (a–i) Micrographs showing the AFM height (a–f) and phase (g–i) of a gelatin film's surface before (right) and after (left) it was subjected to ultrapure water vapors through C-SVA. Following the exposure to ultrapure water vapors, the gelatin films exhibit a structure with

granular-like, elongated shapes that are randomly spread across the entire surface. Image reproduced with permission from ref. [1].

### 3.3 Dextrin's microstructural alteration

Dextrin was another biopolymer exposed to ultrapure water solvents with the help of the C-SVA method. The optical micrographs presented in Figures 4a and 4b, taken of a dextrin film prior to and following its processing, clearly illustrate that the C-SVA processing led to a reorganization of the dextrin chains. Such changes occurred in regions of the film that underwent dewetting, a phenomenon that arose due to the unstable nature of the dextrin film under the conditions of C-SVA processing. Figure 4a emphasizes the resulting morphology of a typical dewetting pattern, exhibiting an average diameter of about several hundreds of micrometers. Obviously, no such patterns were observed on the unexposed dextrin film (Figure 4b), suggesting that the latter became unstable upon C-SVA processing. Nonetheless, when the morphologies of the exposed and unexposed dextrin films were more closely examined with AFM, it was noted that both shapes were smooth and featureless at the micrometer level (Figure 4c,d). Yet, at a smaller scale, there were noticeable differences between the two shapes (Figure 4e–j). As it was inferred from the high-magnification AFM phase micrographs by analyzing many cross-sectional profiles, the substructures forming inside the dewetted pattern (three such substructures are indicated by the dotted rectangular shape in Figure 4i) had an average lateral dimension of about 41 ± 5 nm. . In comparison, the lateral dimension of substructures observed on the unprocessed dextrin film (three such substructures are indicated by the dotted rectangular shape in Figure 4j) was only around 25 ± 5 nm. This observation could be possibly explained by assuming that the elongated shape observed could be due to the dextrin chains adopting a wider arrangement, after

undergoing C-SVA processing and then experiencing dewetting, which led to a conformation that is less folded compared to a regular conformation. Finally, it is important to note that various microstructures of dextrin, primarily associated with film configurations, have been previously documented in the literature. These include different forms such as powder-based granular [95] and egg-like [96] morphologies, smooth and featureless surfaces [97], [98], homogeneous and/or non-porous [47] structures, as well as spherical and branched [99] shapes.

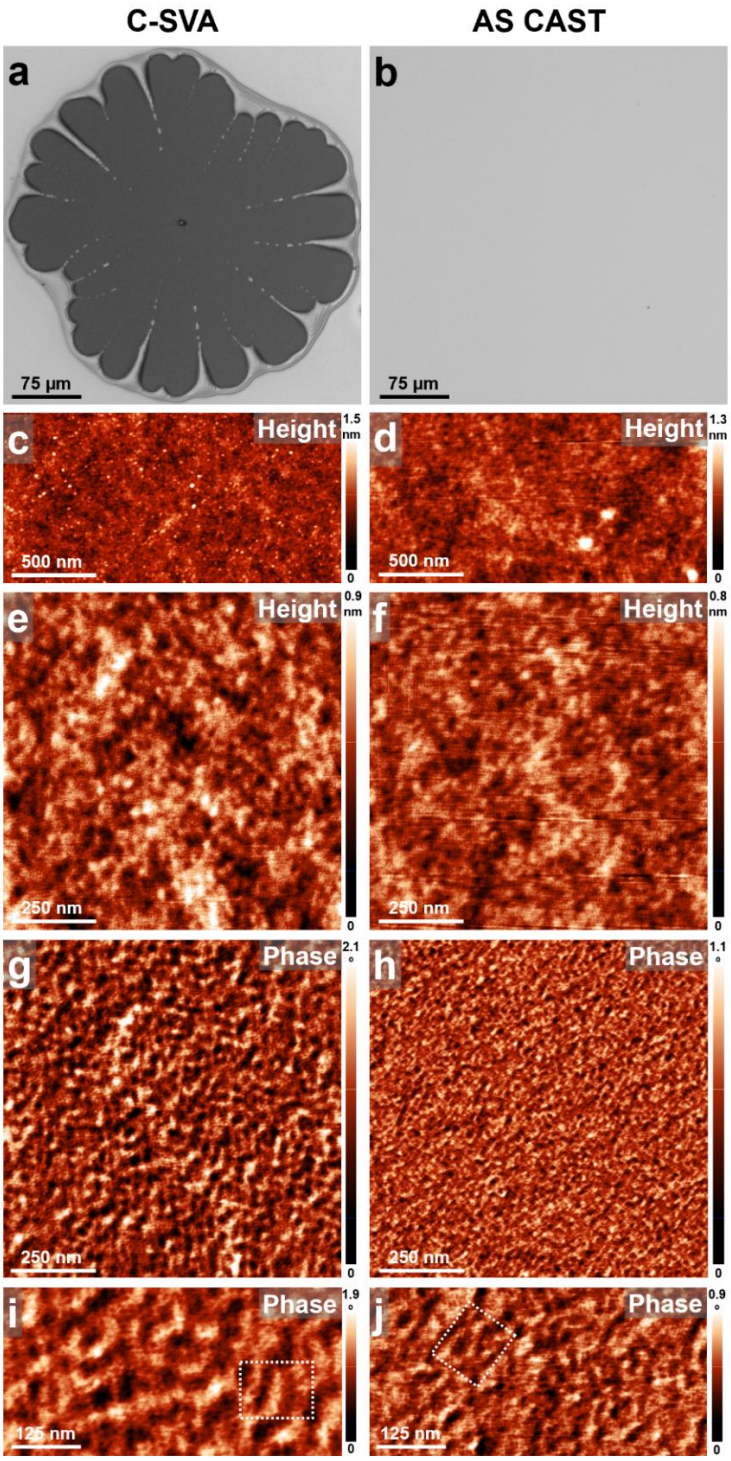


**Figure 5.** (a–j) Optical (a,b) and AFM height (c–f) and phase (g–j) images showing the surface morphology of a thin film of dextrin before (right side) and after (left side) being exposed to ultrapure water vapors via C-SVA. Note that the substructures forming inside the dewetted pattern in (a) had an average lateral dimension much larger than the substructures observed on the unprocessed dextrin film in (b). The dotted shapes in (i,j) are for guiding the eye only. Image reproduced with permission from ref.[1].

### 3.4 Glycogen, chitosan and phytagel based nanostructures

Opposite to dextrin, overall, glycogen molecules did not form significant crystalline formations (Figure 5). The glycogen's reference film surface appeared to be smooth and uniform, similar to the sample that was exposed to water vapor through the C-SVA technique (Figure 4a–h). The surfaces of both probes were dense, with only a few small pores scattered throughout, and showed a roughness at the nanometer level. However, upon closer examination of the AFM phase images at higher magnifications, it was noted that the glycogen molecules may have adopted a slightly different chain conformation upon C-SVA processing in water vapors, as compared with the glycogen chains that generated the reference film. More precisely, while the glycogen structures formed at the molecular level displayed a rather lamellar appearance in both cases, their average lateral dimension (e.g., width) was smaller within the film that was processed via the C-SVA (about 9.4 ± 1 nm), as compared with the average dimension of structures formed within the unexposed reference film (~13.5 ± 2 nm in width; see Figure 5i,j). Interestingly, in both films, the observed lamellae seemed to comprise spherical objects of an average diameter of about 9.4 ± 1 nm and 13.5 ± 2 nm, respectively. As no proof for crystallization was found using the optical microscopy and AFM techniques, we temporarily reached the conclusion that the observed glycogen structures were a result of the self-assembly process that packed glycogen chains into small nanoparticles and then further arranged the latter into curved, lamellar rows. Our results match closely with the earlier theoretical and experimental studies that showed a tendency for glycogen molecules to aggregate into nanoparticles [36], [100], [101]. Such nanoparticles are generally a result of randomly joined glycogen branches (of a typical dimension of about 2 nm) that form so-called β-bonds (typically exhibiting a size of ~20 nm) at a larger scale, which in turn can join again on an even larger scale to form ~100

nm sized $\alpha$-bonds[36], [102], [103], [104]. Judging by the size of our glycogen nanoparticles, although sensitively smaller, they would still fit within the case of typical β-particles (most probably displaying less branching after the processing in ultrapure water vapors via the C-SVA; compare the particle diameters of 9.4 ± 1 nm and 13.5 ± 2 nm). These latter β-particles most probably failed to further form larger $\alpha$-particles and instead preferred to line up into curved lamellar structures, as observed in Figure 5i,j.

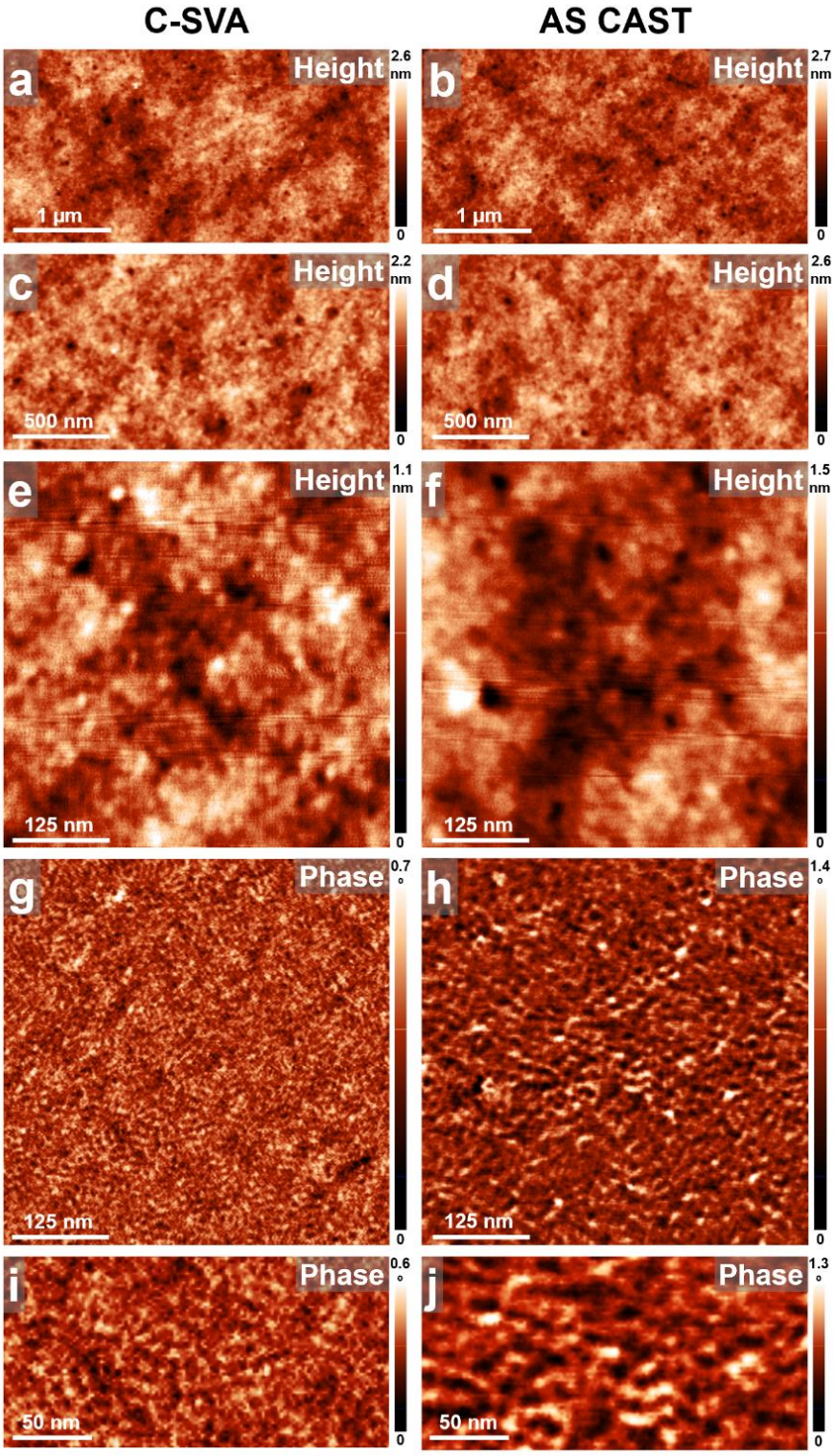


**Figure 6**. (a–j) AFM height (a–f) and phase (g–j) micrographs illustrating the surface morphology of a thin film of glycogen before (right side) and after (left side) being exposed to ultrapure water vapors via the C-SVA method. The surface morphology of both C-SVA processed and unprocessed reference films comprised spherical objects of an average diameter of ~9.4 nm and

~13.5 nm, respectively. Note that artifacts such as some noisy lines in (e,f) cannot be avoided during the AFM measurements conducted while using weak tapping forces (i.e., a very soft tapping mode regime) and are rather normal, especially when acquiring high magnification AFM images of a rather small surface area. Image reproduced with permission from ref.[1].

Chitosan is another biopolymer known to form nanoparticles[105], [106], [107] as well as mono and multi-chamber vesicles [108]. It is a well-study biopolymer and, consequently, it has a vast range of applications counting from biotechnology to pharmaceutics and medicines, membranes and water treatment, cosmetics and foods [109], [110]. Therefore, there is a lot of interest in altering and manipulating its corresponding film microstructure. According to various scientific reports, the latter is generally represented by a homogenous smooth and featureless surface [111], [112], [113], [114], often exhibiting granular [115] or spherical structures [116], [117]. However, the arrangement of chitosan at the microscale in thin films was demonstrated to be highly influenced by the film casting conditions and the type of utilized substrate. As a result, chitosan can form uniform network structures composed of fine chains, spherical nanoparticles, dendritic structures, branched chains, or other dense networks comprising small particles [118]. Comparing our results obtained on chitosan films with those reported in the literature, we can indeed confirm that the chitosan molecules usually arranged themselves into round shapes that spread across the entire film surface immediately after the spinning casting was complete (Figure 6, right side). Moreover, the film surface appeared smooth and featureless in lower magnification AFM height images. The average diameter of spherical structures, better visible in Figure 6f,h (and emphasized in the ellipsoidal dotted shape in Figure 6h), was determined to be around 10 ± 1 nm. Interestingly, while

the film surface remained smooth and featureless also upon processing the chitosan film in acetic acid vapors via the C-SVA method (see the low-magnification AFM height and phase images in Figure 6a,c,e), a closer view with the AFM technique revealed that the spherical chitosan structures further assembled into more or less straight lamellar rows (several such rows are clearly delimited within the rectangular dotted shape in Figure 6h) of an average width of only 7 ± 1 nm, just like it was previously observed in the case of glycogen.

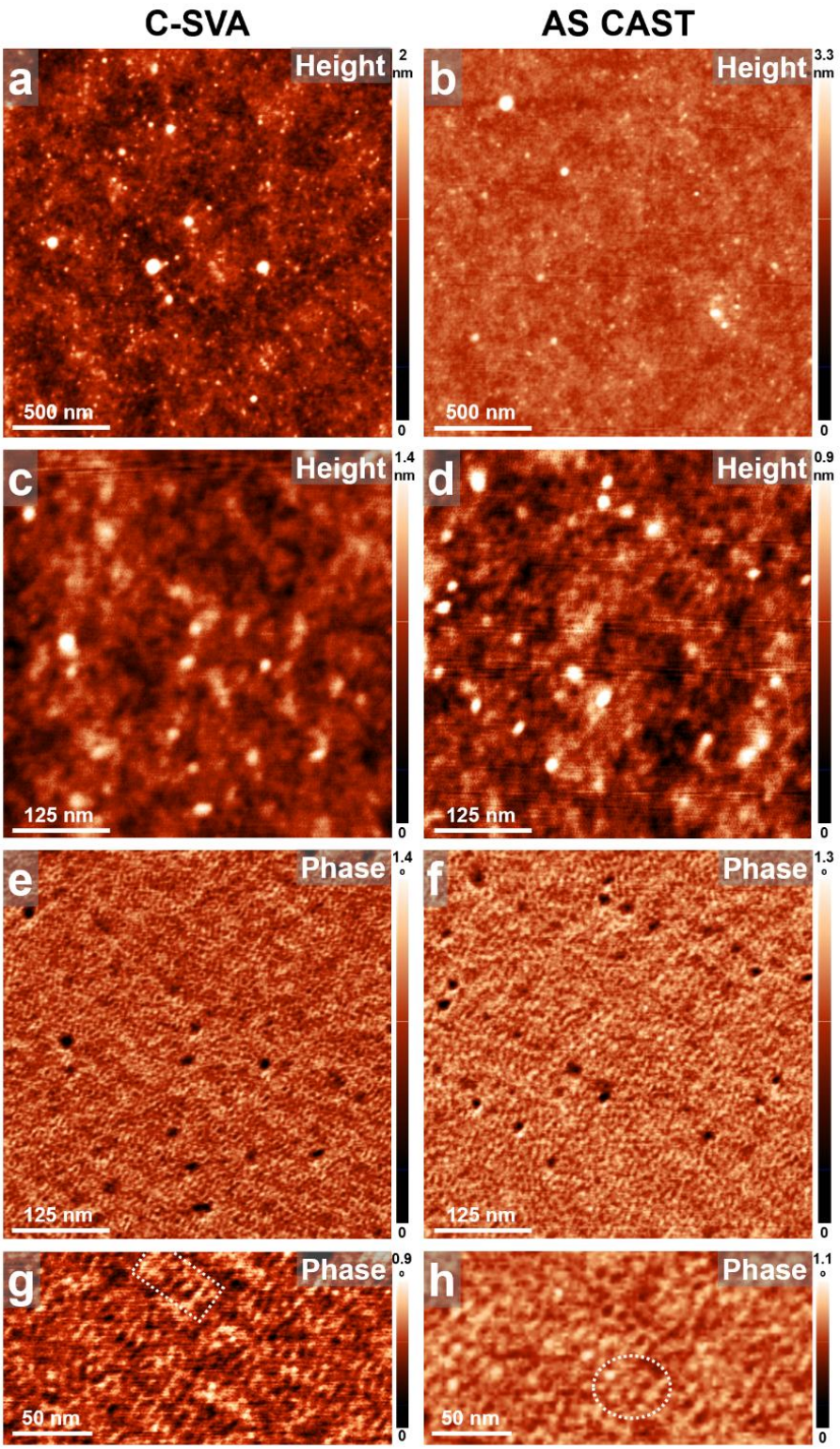


**Figure 7**. (a–h) AFM height (a–d) and phase (e–h) micrographs depicting the surface morphology of a thin film of chitosan before (right side) and after (left side) being exposed to acetic acid vapors via the C-SVA method. The dotted shapes in (g,h) are for guiding the eye only. Note that the surface morphology of chitosan changed upon C-SVA processing in acetic acid vapors from

random ~10 nm large spherical structures to smaller spherical structures often assembled into rather straight lamellar rows. Also note that artifacts such as some noisy lines in (c,d) cannot be avoided during the AFM measurements conducted while using weak tapping forces (i.e., a very soft tapping mode regime). Image reproduced with permission from ref.[1].

Furthermore, we also conducted extended AFM studies on thin films of phytagel (also known as gellan gum) molecule. The results are presented in Figure 7. It was observed that the C-SVA processing did not alter the structure of the film for this specific biomolecule. The film's surface appeared smooth and tightly packed, showing no distinct patterns at the micrometer scale when compared between the left and right sides of Figure 7. Despite this, we decided to include the corresponding AFM images, as they offer a detailed view of the phytagel system and demonstrate that the phytagel molecules naturally organize into thin, helical structures with an average width of about 11 ± 2 nm and a height of a few nanometers (see one of such structures emphasized in Figure 7j in between the two dotted white lines).To the best of our knowledge, these helix-resembling structures of phytagel systems in the thin film configuration were not visualized in such detail in the literature until now. While a crystal structure of gellan was deciphered by means of X-ray diffraction and shown to comprise three-fold helical chains assembled in parallel with each other in an intertwined duplex, with each chain being translated half a pitch with respect to the other [119], only low-magnification AFM images depicting phytagel fibrils and fibrillar networks were reported [120], [121], [122], [123]. It was proposed that these phytagel fibrils could be created by first organizing single chain phytagel molecules into structured double helices, which then combined to form interhelical connections [120]. Also further note that, while some higher structures appeared darker (e.g., softer) in the phase images (see the dotted circular shapes in Figure 7f,h), these structures were featureless (i.e., no helical

structures were present), and thus most probably comprised soft amorphous/coiled-like molecular arrangements. Moreover, taking into account all these data and considering that fibrous structures of cross-sectional heights around 1 nm are considered to consist of bundles of laterally aggregated double helices [122], we tentatively suggest that the 11 ± 2 nm wide and few nanometers tall helix-resembling structures of phytagel shown in Figure 7 represent interhelical associations of double-helix bundles.

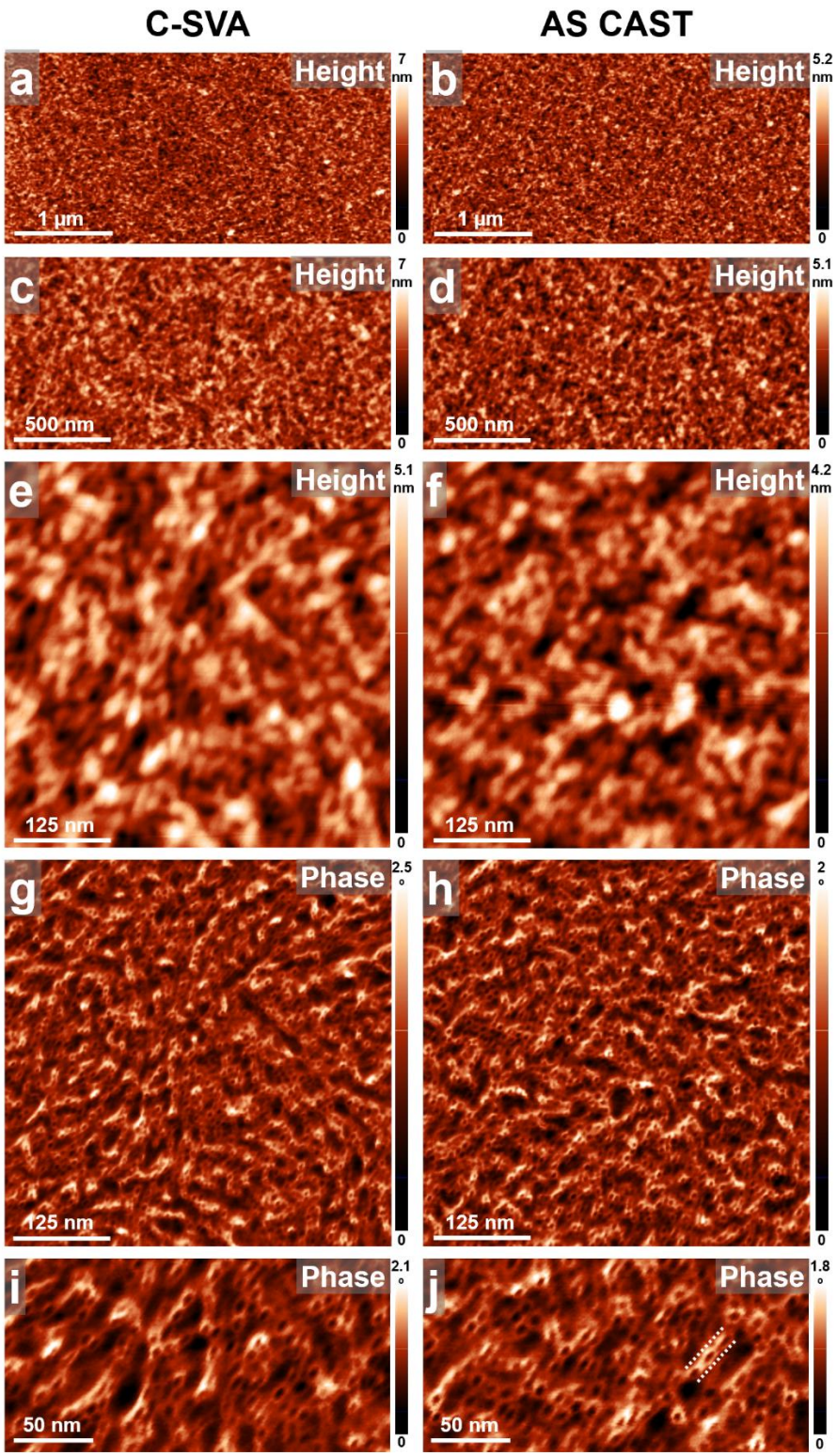


**Figure 8**. (a–j) AFM height (a–f) and phase (g–j) micrographs depicting the surface morphology of a thin film of phytagel before (right side) and after (left side) being exposed to ultrapure water vapors via the C-SVA method. In (i,j), interhelical associations among bundles of double helices can be observed. Note that while a few noisy artifact lines in (e,f), indicated by the white arrow,

could not be avoided while acquiring the AFM height images, these lines are rather normal when performing AFM measurements in a very soft tapping mode regime (employing weak tapping forces) over a rather small area. The dotted circular shapes in (f,h), as well as the dotted arrows in (e,f) and lines in (j), are for eye guidance only. Image reproduced with permission from ref.[1].

## 3.5 Structuring poly-dopamine

Dopamine hydrochloride was the last biological monomeric system that we processed in ultrapure water vapors using the C-SVA method and further investigated for surface microstructure with the AFM technique (see the obtained results summarized in Figure 8). Right after the spin-casting of thin dopamine hydrochloride films, under the optical microscope, we observed that many columnar dendritic structures self-assembled all over the film surface (Figure 8b). The dendritic columns were distinctly separated by visibly empty spaces. Upon closer examination using the AFM technique, the reference dopamine film revealed numerous amorphous areas interspersed with more rigid crystalline columnar branches (Figure 8d,f). Plausibly, the delimitation of columnar branches by the large empty areas (better visible in Figure 8h) was a result of the competition between the neighboring self-assembling dendritic branches for the available molecules in the surrounding volume. Furthermore, the majority of dendritic columnar branches was characterized by highly crystalline and very rigid margins, as can be observed from the AFM phase image presented in Figure 8j. Here, these margins displayed a very bright color. Unfortunately, because of (i) the intense contrast, (ii) the large variations in height across lateral dimensions smaller than 500 nm displayed on the surface of this reference film, and (iii) the highly presence of some amorphous/sticky molecules on top of the columnar branches (amorphous molecules were often sticking to the AFM tip), it was not possible to image such branches clearly at a higher AFM magnification than that presented in Figure 8h,j. The columnar dendritic structure is not a novel element

in dopamine research. It is already known it the literature that (columnar) dendrites, spoke-like, flower-like, or various fractal-like structures can be self-assembled from polydopamine [124]. It's important to note that under specific pH and temperature conditions, or when combined with certain assisting materials (chemical groups), dopamine is known to self-polymerize, leading to the formation of what is referred to as polydopamine[124], [125], [126]. Given that we utilized ultra-pure water as a solvent in our experiments, which was bubbled with nitrogen gas and caused an average pH of 7 [127], it was anticipated that our starting material, dopamine hydrochloride, would self-polymerize into polydopamine. Also, it was expected to undergo self-assembly during the brief deposition time associated with spin casting (as illustrated on the right side of Figure 8). Therefore the columnar dendritic structures presented in Figure 8 are, for instance, similar to the structures reported not long ago by Zhang and co-workers[124].

The novelty of investigating polydopamine films emerged when we advanced our approach by exposing these films to ultrapure water vapors using the C-SVA method. This exposure resulted in the formation of more compact columnar dendritic structures (as depicted in the optical micrograph in Figure 8a). Notably, there were no longer large empty regions between the columnar branches, indicating that polydopamine molecules with enhanced mobility could move freely within the enriched, swollen "film solution" and efficiently reach the "structure assembling site." This observation was further supported by the AFM height micrographs shown in Figure 8c,e. However, very narrow gaps separating the self-assembled compact branches were only observable in the high-magnification AFM height and phase images shown in Figures 8g and 8i. Furthermore, because of the more compact structure of the branches, it was possible to identify at least 1 × 1 $\mu m^2$ large areas that were very smooth and not covered with any detectable (amorphous) sticky molecules (see one of such areas

delimited by the dotted square shape in Figure 8i). Consequently, we successfully obtained high-magnification AFM images, revealing new insights into the microstructure of polydopamine (see Figure 9). Notably, as depicted in Figure 9c, the polydopamine system self-assembled into curved lamellar-like structures with an average lateral dimension of approximately 8 ± 1.5 nm. This value was inferred from the analysis of several cross-sectional profiles
taken along various directions in Figure 9c, and it was significantly smaller than the value of granular features (displaying a diameter of 25 ± 5 nm [99], similar [101], or larger [102,103]) commonly reported in the literature. To the best of our knowledge, no lamellar-resembling structures of polydopamine were reported before and depicted at this magnified scale.

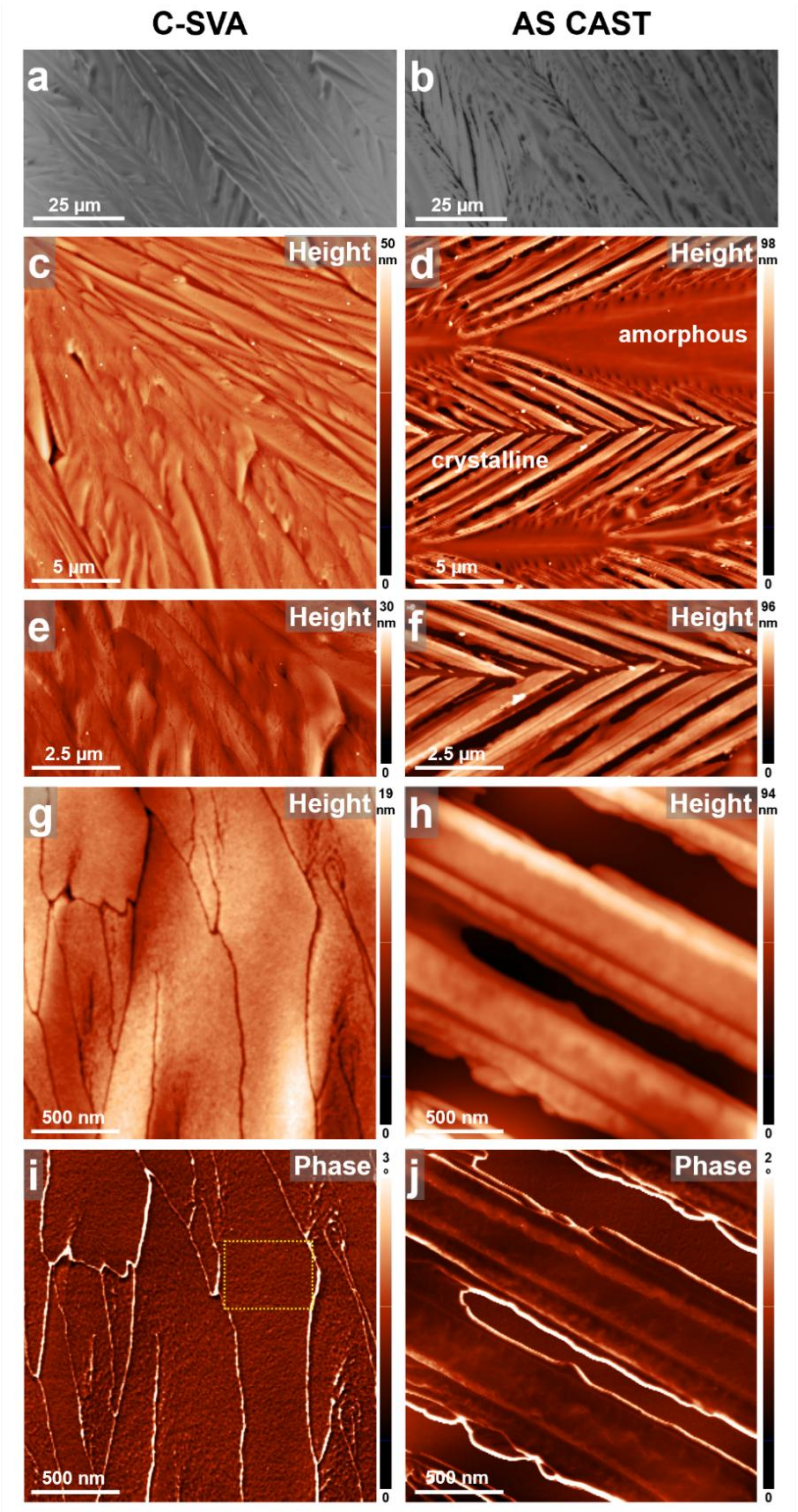


**Figure 9**. (a–j) Optical (a,b) and AFM height (c,h) and phase (i,j) micrographs illustrating the surface morphology of a thin film of dopamine hydrochloride before (right side) and after (left side) being exposed to ultrapure water vapors via the C-SVA method. More compact columnar dendritic structures, with almost no amorphous material, were obtained upon processing

dopamine via the C-SVA method. The dotted shape in (i) indicates the area that was further magnified in the next Figure 10. Image reproduced with permission from ref.[1].

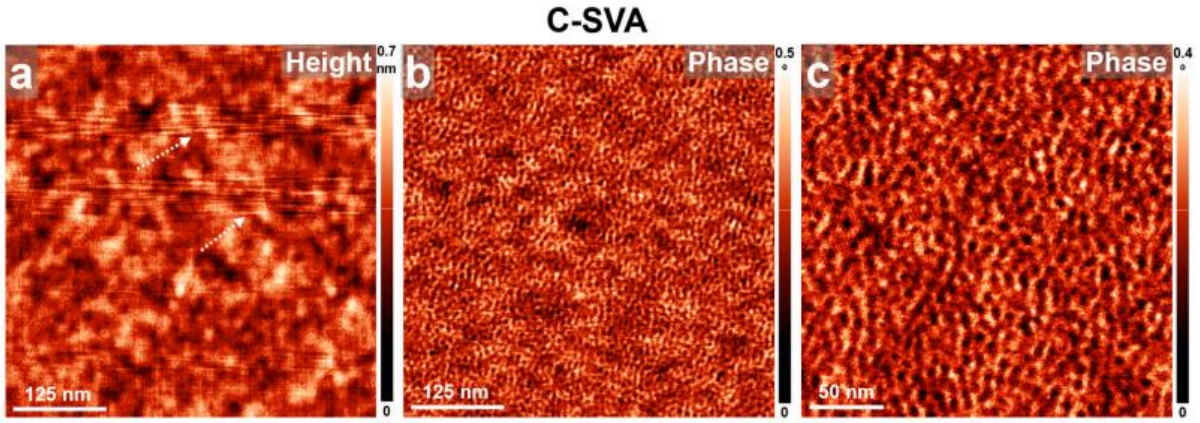


**Figure 10**. (a,b) High-detail AFM height (a) and phase (b) micrographs illustrating the lamellar resembling surface morphology self-assembled in a thin film of dopamine hydrochloride that was exposed to ultrapure water vapors via the C-SVA method. (c) AFM phase image zooming in a region of (b). Note that some noisy artifact lines in (a), indicated by dotted white arrows, could not be avoided while acquiring the AFM height image in a very soft tapping mode regime (and employing weak tapping forces) over a rather small, yet very uniform area. These artifacts are much less prominent in the corresponding phase image and do not impact the obtained AFM results. Image reproduced with permission from ref.[1].

## 3.6 Conclusion

In this chapter, we exposed thin films of various biopolymers, such as gelatin, dextrin, glycogen, chitosan, and phytagel to solvent vapors until a rich film-swelling regime was attained. Biopolymer molecules showed enhanced mobility in this regime and a tendency to crystallization or self-assemble into a variety of forms consisting of highly organized chain conformations. The gelatin biopolymer favored to crystallize into granular compact forms, as the AFM experiments demonstrated. In the cases of glycogen and chitosan, the other biopolymers under study self-assembled into structures that resembled curved

lamellar structures made of spherical nanoparticles, or they took on more intricate helix-like morphologies (in the case of phytagel). The AFM studies presented here are important because they either report novel surface structures of biopolymers (e.g., crystals of gelatin) or depict, in unprecedented detail, surface morphologies composed of interhelical associations of bundles of double phytagel helices.

NOTE: Parts of the text from this theoretical chapter were utilized/adapted from the article that was previously published by us: [1]

# Chapter 4

# Altering poloxamers' morphologies through C-SVA processing

## 4.1 Short summary

Although poloxamers are non-biological polymers, they are used in the medical research and industrial field as bio-compatible substances. Due to their polymeric nature, poloxamers can be processed through spin-casting and C-SVA techniques, much like the previously mentioned bio-polymeric systems. In this chapter are presented figures created under the optical microscope and AFM measurement of poloxamer 188 and 407 films. Every figure is supported by an in-depth analysis and explanation, incorporating relevant theories that utilize the concept of grain boundaries commonly discussed in the literature.

The grain boundary serves as a divider between two crystals (grains) of the same phase that have different orientations relative to each other. This indicates the presence of a transitional area between the grains, where the atomic arrangement deviates from the standard lattice positions [128], [129]. In the case of film solutions casting on surfaces, the presence of multiple nucleation points, characteristic of a high mobility state such as the liquid state, can lead to the formation of grain boundaries.

## 4.2 Poloxamer 188 and 407

For poloxamer 407, AFM images revealed scaly structures both prior to and following C-SVA processing, as observed in Figure 10. One may discern a primary

difference between the two samples (spin-cast and C SVA) at the level of their regularity by closely examining their grain boundaries. This difference makes it evident that self-assembly processes have caused a redistribution of molecules. The processed film displays regular grain boundaries that divide scally-like crystals of very similar sizes and orientations. Although the molecules had multiple nucleation centers, which is the reason for the appearance of the boundaries, the processing method forced them to follow the same direction growth. The processed film demonstrates a higher density of structures, showcasing a smaller and compact arrangement. Due to their nano-scale dimensions measuring at 550 ± 200 nm, the specific shapes are not discernible under an optical microscope. However, the regularity can be seen even at the microscopic level (see figure 10a), where molecules form disc shapes that are clearly divided by large regular borders.

In contrast, grain boundaries are irregular in figure 10d, where there is more extensive crystallization occurring in erratic orientations and sizes.
More precisely, the reference film displays various, relatively large, cell-like morphologies that can be clearly observed with an optical microscope (Figure 10 b) with the smallest diameter measured around 2.5 ± 0.25 μm (Figure 10 d), each of them orientated in different directions. The size difference supports the hypothesis that, initially, the density of crystallization nuclei for the probe was lower than in its refined state, showcasing another example of when the self-assembly process employs a unitary organization pattern throughout the entire substance.

Within phase measurements, the same boundary-scattered surface, distinctively attributed to the processed probe, can be observed on a scale of just a few nanometers, as shown by the outlined rectangle in Figure 10 i. At that level, the borders become much larger, with surfaces similar to the scales they define. As a result, these boundaries may appear to be a random alternation between the

amorphous material and the crystalline grains, that confer the high mobility of the latter. This mobility conferred by the amorphous network of boundaries at the nanometric level is the main difference between figures 10 i and j. The measurements of the unprocessed substance's phase in figure 10 j make it evident that incomplete grain boundaries exist at the nanometric level (highlighted by the outlined rectangle), but that they are delineating a surface considerably smaller than the grains themselves, leaving less space between molecules and reducing the number of degrees of freedom. Recalling the fractal pattern, which is also present in the Poloxamer 407 crystallization morphology, we propose that this mobility of the crystals caused this soft-almost liquid aspect of the disc-shaped substrate at the optical microscope level, in figure 10 b. The same substrate that is unprocessed has a much stiffer appearance in figure 10a.

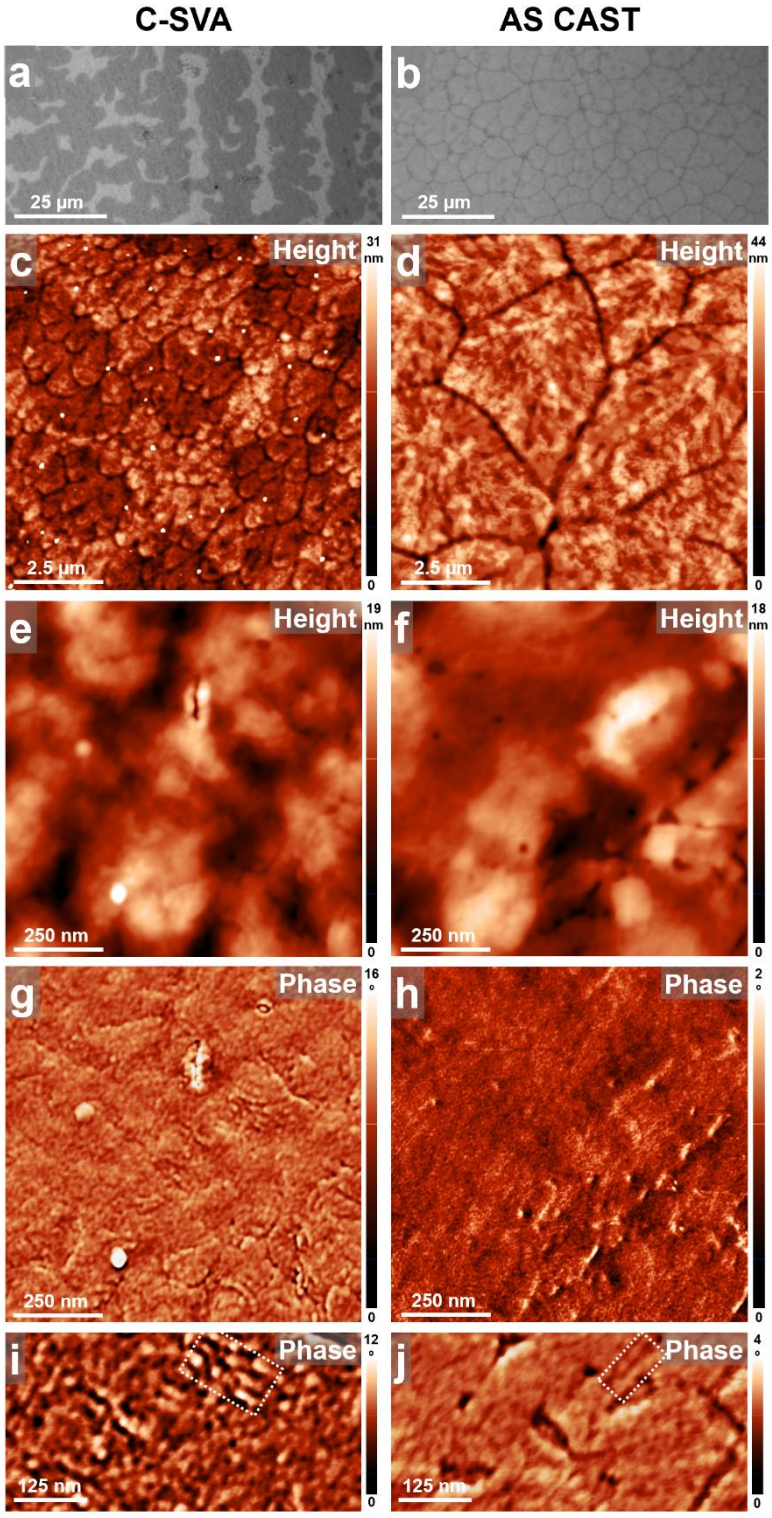


Figure 11. Optical micrographs (a,b) and AFM height (c,f) and phase (g,j) images depict the surface morphology of a thin film of Poloxamer 407, showcasing the condition before (right side) and after (left side) exposure to ultrapure water vapors through the C-SVA method. Following the exposure to ultrapure water vapors, the flake-like structures seen in the unprocessed film

undergo resizing and reorganization, resulting in a compact layer that is uniformly distributed, with the flakes aligned in a similar direction. The dotted shape in (i) and (i) indicates that the difference between the two films phase lies in the amorphous substance abundance that forms a boundary network in the processed film.

Similar to the earlier polymer, the poloxamer 188 film undergoes structural changes during the swelling process in ultrapure water vapor via the C SVA technique, resulting in the development of flake-like structures. Figure 11 a provides an overview highlighting the consistent formation of these structures across the entire surface of the processed film, demonstrating a continuous pattern without any interruptions of amorphous or vacant areas. Going in detail, figure 11 c and e, presents the particularities of these crystallized forms, their average dimensions, width of 350 ± 100 nm or length of 950 ± 300 nm, and makes it evident the existence of the grain boundaries, specific indicators of crystallization. Despite poloxamers 407 and 188 having similar shapes and sizes in their processed forms at some levels of magnitude, their reference films varied significantly, even though both were subjected to the same spin casting technique. At first , the surface of the poloxamer 188 film, shown in Figure 11b, resembled as an amorphous mass primarily oriented in a single direction. While this observation aligns with what we might anticipate based on fluid mechanics and the casting method used, a closer examination of the enhanced images in Figures 11d and 11f reveals an intricate intertwining lamellar structure. In response to these findings, we propose the hypothesis that the film surface is formed by the same scaly-like structures exposed on the surface of the C-SVA processed film, but they have been stacked together and orientated at an angle to the horizontal plane. In this case, the lamellar and apparently straight boundaries, seen more

clearly in the phase measurements (Figure 11h, j), would be just the peaks of the flakes measured by the AFM tip. Furthermore, by examining the uniformity of the color in the phase images, which is somewhat affected by the contrast induced by the peaks, we can deduce that the surface of the flakes maintains their consistency across the analyzed region, with exception at the edges where it abruptly hardens. In contrast, in Figure 11g, i, the processed film flakes surfaces are as stiff as their edges. In addition, in figure 11i we can observe an alternation of hardness through a point-like pattern, giving the impression that the film would have a very rough texture. is currently no AFM measurements published, similar to ours, that support the theoretical basis for this adherent properties.

It is worth mentioning that poloxamer 407 and 188 are predominantly utilized in research as additives, mostly stabilizers [130], [131], [132], [133], [134], [135]. Consequently, there are limited studies focusing on their morphologies. The existing research indicate a dendritic structure [136], [137], [138], which differs significantly from what we are presenting, both in terms of shape and quality. To the best of our knowledge, such a thorough examination of the structure of poloxamer 188 and 407 has not been reported elsewhere.

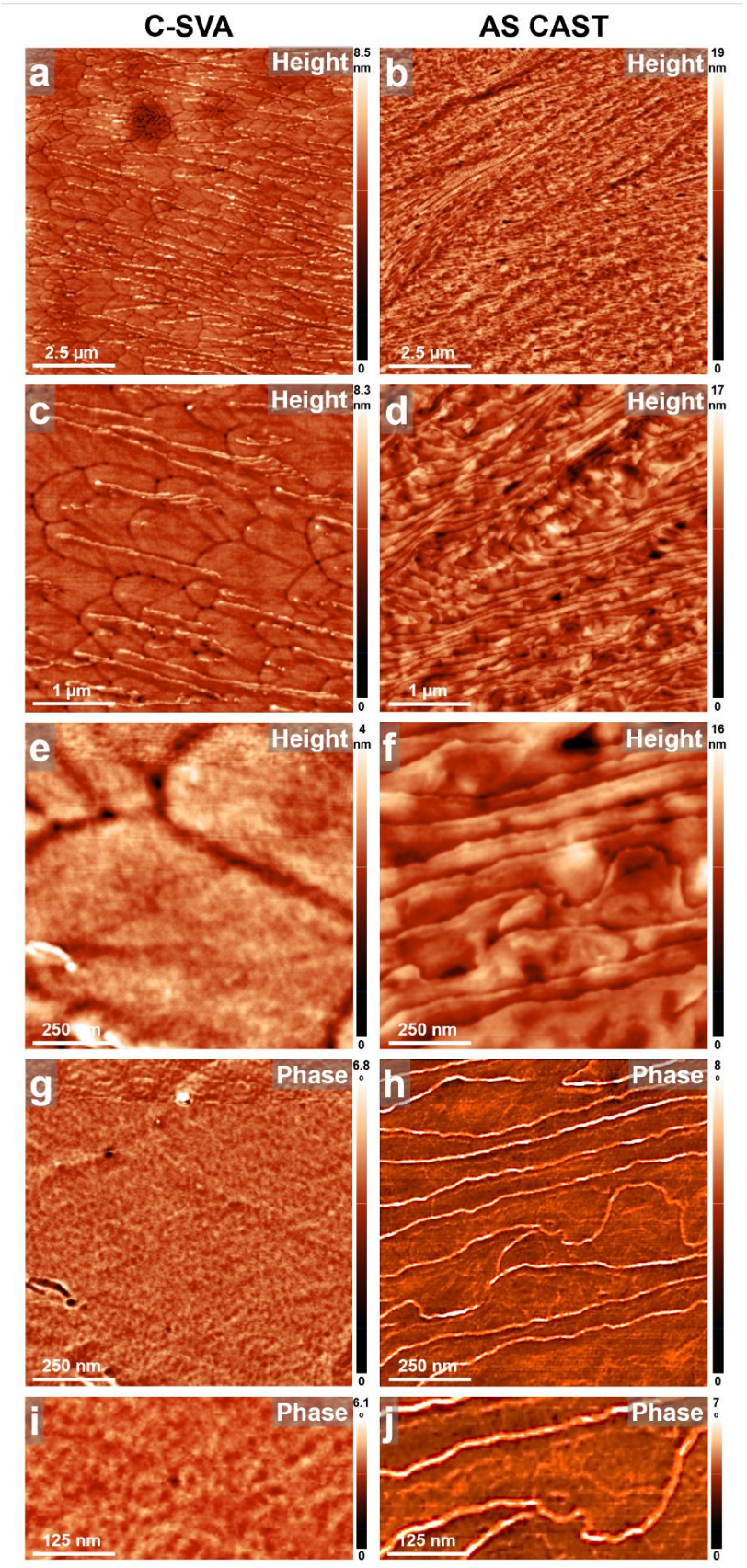
C-SVA
AS CAST
a
Height
8.5
nm
0
2.5 µm
b
Height
19
nm
0
2.5 µm
c
Height
8.3
nm
0
1 µm
d
Height
17
nm
0
1 µm
e
Height
4
nm
0
250 nm
f
Height
16
nm
0
250 nm
g
Phase
6.8
°
0
250 nm
h
Phase
8
°
0
250 nm
i
Phase
6.1
°
0
125 nm
j
Phase
7
°
0
125 nm

Figure 12. (a–j) AFM height (a–f) and phase (g–j) micrographs illustrating the surface morphology of a thin film of poloxamer 188 before (right side) and after (left side) being exposed to ultrapure water vapors via the C-SVA method. The unprocessed film showcase staked flakes on top of each other and oriented at an angle to the horizontal plane, that create the illusion of lamellar narrow structures. After processing the poloxamer 188 film, a compact scally-like pattern is formed, similar with the poloxamer 407 refined morphology.

## 4.4 Conclusions

In this chapter, we subjected thin films of poloxamer 407 and 188 to solvent vapors until we achieved a notable stage of film swelling to induce a self-assembly phenomenon. The triblock copolymers appeared to exhibit similar scaly-like structures; however, a more detailed examination revealed the unique characteristics of each one. The poloxamer 407 processed film exhibits a surface characterized by prominent grain boundaries at all magnification levels, the figures emphasizing the fractal characteristics of this polymer. In the case of poloxamer 188, it is the unique characteristics of the unprocessed film that stand out. The familiar scaly structures are arranged in a stacked formation, positioned at an angle relative to the horizontal plane. To the best of our knowledge, such a thorough examination of the structure of poloxamer 188 and 407 has not been reported elsewhere.

# General Conclusions

This study explores the connection between the substance's microstructure and its processing methods by showcasing novel (bio)polymeric morphologies obtained through C-SVA processing technique. This method involved exposing thin films made from different biopolymers such as dextrin, glycogen, and phytagel, along with poloxamer films like P407 and P188, to solvent vapors in order to generate quasi-solution from swelling the films. In this environment, the molecules showed greater mobility, which led to a higher tendency for crystallization or self-assembly into diverse structures with more orderly chain conformations. Findings from the AFM studies reveal that the dextrin biopolymer underwent a dewetting process, which caused the emergence of flower-like craters on the film surface. These results enhance our understanding of the complexities associated with dewetting phenomena. The other biopolymers analyzed self-assembled into various structures: glycogen formed curved lamellar structures with spherical nanoparticles, while phytagel exhibited more complex helix-like morphologies. Furthermore, the processing of poloxamer P188 films revealed a three-dimensional surface restructuring, with the reference film displaying structures that were angled to the horizontal surface and flattened through processing.

Moreover, while the efficiency of the rich swelling of thin (bio)polymeric films in solvent vapors was demonstrated some time ago on various polypeptide homopolymers, diblock, and hetero-arm star block copolymers (see ref. [81], [82]), the optimization of this processing method to C-SVA gave us the ability to alter and control the morphology of other diblock and triblock copolymers (see ref. [80]) with the help of both self-assembly and crystallization processes. In all these studies, one has to be aware that while the process of film

swelling is the same no matter which polymeric system is processed (e.g., condensation of warmer solvent vapors on the colder film surface), the physical parameters like the film temperature when the condensation starts or the amount of condensed solvent vapors, critically depend on the type of utilized solvent (and thus, on its volatility), on its temperature or the amount of vapors introduced in the sample chamber. Therefore, some limitations of the here-proposed C-SVA tool are related to the use of solvents with very low volatility that would require condensation to happen at temperatures lower than 10–12 ◦C or of bad solvents unable to fully dissolve the polymer film, thus failing to generate a homogeneous film solution. This work further completes the spectrum of the applicability of the C-SVA method on certain biopolymers, as well as simple monomer materials (e.g., dopamine hydrochloride), a potential that could be exploited in the future when designing and developing novel biopolymer-based applications, especially when targeting applications highly sensitive to the molecular arrangements such as drug delivery or sensing.

# References


[1] M. Băbuțan and I. Botiz, "Morphological Characteristics of Biopolymer Thin Films Swollen-Rich in Solvent Vapors," *Biomimetics*, vol. 9, no. 7, Art. no. 7, Jul. 2024, doi: 10.3390/biomimetics9070396.

[2] S. V. Patil, S. S. Shelake, and S. S. Patil, "11 - Polymeric materials for targeted delivery of bioactive agents and drugs," in *Fundamental Biomaterials: Polymers*, S. Thomas, P. Balakrishnan, and M. S. Sreekala, Eds., in Woodhead Publishing Series in Biomaterials. , Woodhead Publishing, 2018, pp. 249–266. doi: 10.1016/B978-0-08-102194-1.00011-6.

[3] A. Harugade, A. P. Sherje, and A. Pethe, "Chitosan: A review on properties, biological activities and recent progress in biomedical applications," *Reactive and Functional Polymers*, vol. 191, p. 105634, Oct. 2023, doi: 10.1016/j.reactfunctpolym.2023.105634.

[4] T. Asai, T. Hayashi, K. Kuroki, M. Okano, T. Kiriyama, and T. Kawai, "In vitro biocompatibility of dextrin: the addition of a low concentration of dextrin in the medium promotes the cell activity of L929 mouse fibroblasts," *Cell Biol Int*, vol. 35, no. 6, pp. 645–648, Jun. 2011, doi: 10.1042/CBI20100264.

[5] E. J. Ricci, L. O. Lunardi, D. M. A. Nanclares, and J. M. Marchetti, "Sustained release of lidocaine from Poloxamer 407 gels," *International Journal of Pharmaceutics*, vol. 288, no. 2, pp. 235–244, Jan. 2005, doi: 10.1016/j.ijpharm.2004.09.028.

[6] S. K. Pazhanimala, D. Vllasaliu, and B. T. Raimi-Abraham, "Engineering Biomimetic Gelatin Based Nanostructures as Synthetic Substrates for Cell Culture," *Applied Sciences*, vol. 9, no. 8, Art. no. 8, Jan. 2019, doi: 10.3390/app9081583.

[7] M. Rabyk *et al.*, "Modified glycogen as construction material for functional biomimetic microfibers," *Carbohydrate Polymers*, vol. 152, pp. 271–279, Nov. 2016, doi: 10.1016/j.carbpol.2016.06.107.

[8] I. Botiz, "Prominent processing techniques to manipulate semiconducting polymer microstructures," *J. Mater. Chem. C*, vol. 11, no. 2, pp. 364–405, Jan. 2023, doi: 10.1039/D2TC03971K.

[9] J. Danglad-Flores, S. Eickelmann, and H. Riegler, "Deposition of polymer films by spin casting: A quantitative analysis," *Chemical Engineering Science*, vol. 179, pp. 257–264, Apr. 2018, doi: 10.1016/j.ces.2018.01.012.

[10] T. Biswal, "Biopolymers for tissue engineering applications: A review," *Materials Today: Proceedings*, vol. 41, pp. 397–402, Jan. 2021, doi: 10.1016/j.matpr.2020.09.628.

[11] J. Aggarwal, S. Sharma, H. Kamyab, and A. Kumar, "The Realm of Biopolymers and Their Usage: An Overview," vol. 8, no. 2, 2020.
[12] T. Biswal, S. K. BadJena, and D. Pradhan, "Sustainable biomaterials and their applications: A short review," *Materials Today: Proceedings*, vol. 30, pp. 274–282, Jan. 2020, doi: 10.1016/j.matpr.2020.01.437.
[13] R. Priyadarshi and J.-W. Rhim, "Chitosan-based biodegradable functional films for food packaging applications," *Innovative Food Science & Emerging Technologies*, vol. 62, p. 102346, Jun. 2020, doi: 10.1016/j.ifset.2020.102346.
[14] M. Azmana, S. Mahmood, A. R. Hilles, A. Rahman, M. A. B. Arifin, and S. Ahmed, "A review on chitosan and chitosan-based bionanocomposites: Promising material for combatting global issues and its applications," *International Journal of Biological Macromolecules*, vol. 185, pp. 832–848, Aug. 2021, doi: 10.1016/j.ijbiomac.2021.07.023.
[15] T. Philibert, B. H. Lee, and N. Fabien, "Current Status and New Perspectives on Chitin and Chitosan as Functional Biopolymers," *Appl Biochem Biotechnol*, vol. 181, no. 4, pp. 1314–1337, Apr. 2017, doi: 10.1007/s12010-016-2286-2.
[16] V. Gopinath, S. Saravanan, A. R. Al-Maleki, M. Ramesh, and J. Vadivelu, "A review of natural polysaccharides for drug delivery applications: Special focus on cellulose, starch and glycogen," *Biomedicine & Pharmacotherapy*, vol. 107, pp. 96–108, Nov. 2018, doi: 10.1016/j.biopha.2018.07.136.
[17] S. S. Mehetre, R. K. Shankar, R. K. Ameta, and S. S. Behere, "Chapter 1 - An introduction to protein-based biopolymers," in *Protein-Based Biopolymers*, S. Kalia and S. Sharma, Eds., in Woodhead Publishing Series in Biomaterials. , Woodhead Publishing, 2023, pp. 1–40. doi: 10.1016/B978-0-323-90545-9.00001-X.
[18] M. W. T. Werten, G. Eggink, M. A. Cohen Stuart, and F. A. de Wolf, "Production of protein-based polymers in *Pichia pastoris*," *Biotechnology Advances*, vol. 37, no. 5, pp. 642–666, Sep. 2019, doi: 10.1016/j.biotechadv.2019.03.012.
[19] S. Kapoor and S. C. Kundu, "Silk protein-based hydrogels: Promising advanced materials for biomedical applications," *Acta Biomaterialia*, vol. 31, pp. 17–32, Feb. 2016, doi: 10.1016/j.actbio.2015.11.034.
[20] K. DeFrates *et al.*, "Protein Polymer-Based Nanoparticles: Fabrication and Medical Applications," *International Journal of Molecular Sciences*, vol. 19, no. 6, Art. no. 6, Jun. 2018, doi: 10.3390/ijms19061717.
[21] F. Praetorius, B. Kick, K. L. Behler, M. N. Honemann, D. Weuster-Botz, and H. Dietz, "Biotechnological mass production of DNA origami," *Nature*, vol. 552, no. 7683, pp. 84–87, Dec. 2017, doi: 10.1038/nature24650.

[22] F. Li, J. Tang, J. Geng, D. Luo, and D. Yang, "Polymeric DNA hydrogel: Design, synthesis and applications," *Progress in Polymer Science*, vol. 98, p. 101163, Nov. 2019, doi: 10.1016/j.progpolymsci.2019.101163.

[23] S. Kalia and S. Sharma, *Protein-Based Biopolymers: From Source to Biomedical Applications*. Woodhead Publishing, 2022.

[24] N. Davidenko *et al.*, "Evaluation of cell binding to collagen and gelatin: a study of theeffect of 2D and 3D architecture and surface chemistry," *J Mater Sci: Mater Med*, vol. 27, no. 10, p. 148, Aug. 2016, doi: 10.1007/s10856-016-5763-9.

[25] W. Treesuppharat, P. Rojanapanthu, C. Siangsanoh, H. Manuspiya, and S. Ummartyotin, "Synthesis and characterization of bacterial cellulose and gelatin-based hydrogel composites for drug-delivery systems," *Biotechnology Reports*, vol. 15, pp. 84–91, Sep. 2017, doi: 10.1016/j.btre.2017.07.002.

[26] D. Suresh, A. Suresh, and R. Kannan, "Engineering biomolecular systems: Controlling the self-assembly of gelatin to form ultra-small bioactive nanomaterials," *Bioactive Materials*, vol. 18, pp. 321–336, Dec. 2022, doi: 10.1016/j.bioactmat.2022.02.035.

[27] K. Guillén-Carvajal, B. Valdez-Salas, E. Beltrán-Partida, J. Salomón-Carlos, and N. Cheng, "Chitosan, Gelatin, and Collagen Hydrogels for Bone Regeneration," *Polymers*, vol. 15, no. 13, Art. no. 13, Jan. 2023, doi: 10.3390/polym15132762.

[28] S. Petros, T. Tesfaye, and M. Ayele, "A Review on Gelatin Based Hydrogels for Medical Textile Applications," *Journal of Engineering*, vol. 2020, no. 1, p. 8866582, 2020, doi: 10.1155/2020/8866582.

[29] B. Salahuddin, S. Wang, D. Sangian, S. Aziz, and Q. Gu, "Hybrid Gelatin Hydrogels in Nanomedicine Applications," *ACS Appl. Bio Mater.*, vol. 4, no. 4, pp. 2886–2906, Apr. 2021, doi: 10.1021/acsabm.0c01630.

[30] C. Teijeiro-Valiño *et al.*, "Biocompatible magnetic gelatin nanoparticles with enhanced MRI contrast performance prepared by single-step desolvation method," *Nano Ex.*, vol. 2, no. 2, p. 020011, Apr. 2021, doi: 10.1088/2632-959X/abf58e.

[31] A.-V. Weiss, D. Schorr, J. K. Metz, M. Yildirim, S. A. Khan, and M. Schneider, "Gelatin nanoparticles with tunable mechanical properties: effect of crosslinking time and loading," *Beilstein J. Nanotechnol.*, vol. 13, no. 1, pp. 778–787, Aug. 2022, doi: 10.3762/bjnano.13.68.

[32] G. A. Valencia, E. N. Zare, P. Makvandi, and T. J. Gutiérrez, "Self-Assembled Carbohydrate Polymers for Food Applications: A Review," *Comprehensive Reviews in Food Science and Food Safety*, vol. 18, no. 6, pp. 2009–2024, 2019, doi: 10.1111/1541-4337.12499.

[33] G. M. Mohamed, A. M. Amer, N. H. Osman, M. Z. Sedikc, and M. H. Hussein, "Effects of different gelling agents on the different stages of rice regeneration in two rice cultivars," *Saudi Journal of Biological Sciences*, vol. 28, no. 10, pp. 5738–5744, Oct. 2021, doi: 10.1016/j.sjbs.2021.06.003.

[34] J. Li *et al.*, "Biospecific Self-Assembly of a Nanoparticle Coating for Targeted and Stimuli-Responsive Drug Delivery," *Advanced Functional Materials*, vol. 25, no. 9, pp. 1404–1417, 2015, doi: 10.1002/adfm.201403636.

[35] J. P. Quiñones, H. Peniche, and C. Peniche, "Chitosan Based Self-Assembled Nanoparticles in Drug Delivery," *Polymers*, vol. 10, no. 3, Art. no. 3, Mar. 2018, doi: 10.3390/polym10030235.

[36] Q. A. Besford, F. Cavalieri, and F. Caruso, "Glycogen as a Building Block for Advanced Biological Materials," *Advanced Materials*, vol. 32, no. 18, p. 1904625, 2020, doi: 10.1002/adma.201904625.

[37] L. E. Nita *et al.*, "New Hydrogels Based on Agarose/Phytagel and Peptides," *Macromolecular Bioscience*, vol. 23, no. 3, p. 2200451, 2023, doi: 10.1002/mabi.202200451.

[38] D. Das and S. Pal, "Modified biopolymer-dextrin based crosslinked hydrogels: application in controlled drug delivery," *RSC Adv.*, vol. 5, no. 32, pp. 25014–25050, Mar. 2015, doi: 10.1039/C4RA16103C.

[39] T. Sukpaita, S. Chirachanchai, A. Pimkhaokham, and R. S. Ampornaramveth, "Chitosan-Based Scaffold for Mineralized Tissues Regeneration," *Marine Drugs*, vol. 19, no. 10, Art. no. 10, Oct. 2021, doi: 10.3390/md19100551.

[40] S. D. Kozusko, C. Riccio, M. Goulart, J. Bumgardner, X. L. Jing, and P. Konofaos, "Chitosan as a Bone Scaffold Biomaterial," *Journal of Craniofacial Surgery*, vol. 29, no. 7, p. 1788, Oct. 2018, doi: 10.1097/SCS.0000000000004909.

[41] Y. Kim *et al.*, "Chitosan-Based Biomaterials for Tissue Regeneration," *Pharmaceutics*, vol. 15, no. 3, Art. no. 3, Mar. 2023, doi: 10.3390/pharmaceutics15030807.

[42] Z. Han and G. Liu, "Sugar-based biopolymers as novel imaging agents for molecular magnetic resonance imaging," *WIREs Nanomedicine and Nanobiotechnology*, vol. 11, no. 4, p. e1551, 2019, doi: 10.1002/wnan.1551.

[43] I. Hussain, X. Ma, Y. Luo, and Z. Luo, "Fabrication and characterization of glycogen-based elastic, self-healable, and conductive hydrogels as a wearable strain-sensor for flexible e-skin," *Polymer*, vol. 210, p. 122961, Dec. 2020, doi: 10.1016/j.polymer.2020.122961.

[44] C. N. Jacques, A. K. Hulbert, S. Westenskow, and M. M. Neff, "Production location of the gelling agent Phytagel has a significant impact on Arabidopsis thaliana seedling phenotypic analysis," *PLoS One*, vol. 15, no. 5, p. e0228515, May 2020, doi: 10.1371/journal.pone.0228515.

[45] M. Ishihara, V. Q. Nguyen, Y. Mori, S. Nakamura, and H. Hattori, "Adsorption of Silver Nanoparticles onto Different Surface Structures of Chitin/Chitosan and Correlations with Antimicrobial Activities," *International Journal of Molecular Sciences*, vol. 16, no. 6, Art. no. 6, Jun. 2015, doi: 10.3390/ijms160613973.

[46] N. H. Marei, E. A. El-Samie, T. Salah, G. R. Saad, and A. H. M. Elwahy, "Isolation and characterization of chitosan from different local insects in Egypt," *International Journal of Biological Macromolecules*, vol. 82, pp. 871–877, Jan. 2016, doi: 10.1016/j.ijbiomac.2015.10.024.

[47] G. Nirmala Devi, S. Chitra, S. Selvasekarapandian, M. Premalatha, S. Monisha, and J. Saranya, "Synthesis and characterization of dextrin-based polymer electrolytes for potential applications in energy storage devices," *Ionics*, vol. 23, no. 12, pp. 3377–3388, Dec. 2017, doi: 10.1007/s11581-017-2135-5.

[48] Z. Islamipour, E. N. Zare, F. Salimi, M. Ghomi, and P. Makvandi, "Biodegradable antibacterial and antioxidant nanocomposite films based on dextrin for bioactive food packaging," *J Nanostruct Chem*, vol. 12, no. 5, pp. 991–1006, Oct. 2022, doi: 10.1007/s40097-022-00491-4.

[49] J. S. Patil, S. M. Jadhav, S. V. Mandave, V. Vilegave, and S. B. Dhadde, "Natural Gellan Gum (Phytagel®) Based Novel Hydrogel Beads of Rifampicin for Oral Delivery with Improved Functionality," *Indian Journal of Pharmaceutical Education and Research*, vol. 50, no. 2, 2016.

[50] A. Tejo-Otero *et al.*, "Soft-Tissue-Mimicking Using Hydrogels for the Development of Phantoms," *Gels*, vol. 8, no. 1, Art. no. 1, Jan. 2022, doi: 10.3390/gels8010040.

[51] Y. Xu *et al.*, "Bioinspired polydopamine hydrogels: Strategies and applications," *Progress in Polymer Science*, vol. 146, p. 101740, Nov. 2023, doi: 10.1016/j.progpolymsci.2023.101740.

[52] D. Hauser, D. Septiadi, J. Turner, A. Petri-Fink, and B. Rothen-Rutishauser, "From Bioinspired Glue to Medicine: Polydopamine as a Biomedical Material," *Materials*, vol. 13, no. 7, Art. no. 7, Jan. 2020, doi: 10.3390/ma13071730.

[53] K. Liu, X. Dong, Y. Wang, X. Wu, and H. Dai, "Dopamine-modified chitosan hydrogel for spinal cord injury," *Carbohydrate Polymers*, vol. 298, p. 120047, Dec. 2022, doi: 10.1016/j.carbpol.2022.120047.

[54] A. H. J. Gowda *et al.*, "Design of tunable gelatin-dopamine based bioadhesives," *International Journal of Biological Macromolecules*, vol. 164, pp. 1384–1391, Dec. 2020, doi: 10.1016/j.ijbiomac.2020.07.195.

[55] K. Wang *et al.*, "Dopamine-functionalized poloxamers for antibacterial coating," *Materials Letters*, vol. 291, p. 129591, May 2021, doi: 10.1016/j.matlet.2021.129591.

[56] T.-F. Wu and J.-D. Hong, "Dopamine-Melanin Nanofilms for Biomimetic Structural Coloration," *Biomacromolecules*, vol. 16, no. 2, pp. 660–666, Feb. 2015, doi: 10.1021/bm501773c.
[57] P. Zarrintaj *et al.*, "Poloxamer: A versatile tri-block copolymer for biomedical applications," *Acta Biomaterialia*, vol. 110, pp. 37–67, Jul. 2020, doi: 10.1016/j.actbio.2020.04.028.
[58] A. M. Bodratti and P. Alexandridis, "Formulation of Poloxamers for Drug Delivery," *Journal of Functional Biomaterials*, vol. 9, no. 1, Art. no. 1, Mar. 2018, doi: 10.3390/jfb9010011.
[59] E. Russo and C. Villa, "Poloxamer Hydrogels for Biomedical Applications," *Pharmaceutics*, vol. 11, no. 12, Art. no. 12, Dec. 2019, doi: 10.3390/pharmaceutics11120671.
[60] A. Naharros-Molinero, M. Á. Caballo-González, F. J. de la Mata, and S. García-Gallego, "Direct and Reverse Pluronic Micelles: Design and Characterization of Promising Drug Delivery Nanosystems," *Pharmaceutics*, vol. 14, no. 12, Art. no. 12, Dec. 2022, doi: 10.3390/pharmaceutics14122628.
[61] K. A. Soliman, K. Ullah, A. Shah, D. S. Jones, and T. R. R. Singh, "Poloxamer-based *in situ* gelling thermoresponsive systems for ocular drug delivery applications," *Drug Discovery Today*, vol. 24, no. 8, pp. 1575–1586, Aug. 2019, doi: 10.1016/j.drudis.2019.05.036.
[62] S. Kotta, H. M. Aldawsari, S. M. Badr-Eldin, A. B. Nair, and K. Yt, "Progress in Polymeric Micelles for Drug Delivery Applications," *Pharmaceutics*, vol. 14, no. 8, Art. no. 8, Aug. 2022, doi: 10.3390/pharmaceutics14081636.
[63] A. C. Marques, P. C. Costa, S. Velho, and M. H. Amaral, "Injectable Poloxamer Hydrogels for Local Cancer Therapy," *Gels*, vol. 9, no. 7, Art. no. 7, Jul. 2023, doi: 10.3390/gels9070593.
[64] K. Postolović *et al.*, "Optimization, characterization, and evaluation of carrageenan/alginate/poloxamer/curcumin hydrogel film as a functional wound dressing material," *Materials Today Communications*, vol. 31, p. 103528, Jun. 2022, doi: 10.1016/j.mtcomm.2022.103528.
[65] G. Divyashri *et al.*, "Applications of hydrogel-based delivery systems in wound care and treatment: An up-to-date review," *Polymers for Advanced Technologies*, vol. 33, no. 7, pp. 2025–2043, 2022, doi: 10.1002/pat.5661.
[66] N. Cui *et al.*, "Poloxamer-Based Scaffolds for Tissue Engineering Applications: A Review," *Gels*, vol. 8, no. 6, Art. no. 6, Jun. 2022, doi: 10.3390/gels8060360.
[67] V. N. V. A. Uppuluri, S. Thukani Sathanantham, S. K. Bhimavarapu, and L. Elumalai, "Polymeric Hydrogel Scaffolds: Skin Tissue Engineering and

Regeneration," *Adv Pharm Bull*, vol. 12, no. 3, pp. 437–448, May 2022, doi: 10.34172/apb.2022.069.
[68] Y. E. Park *et al.*, "Sustained Delivery of Lactoferrin Using Poloxamer Gels for Local Bone Regeneration in a Rat Calvarial Defect Model," *Materials*, vol. 15, no. 1, Art. no. 1, Jan. 2022, doi: 10.3390/ma15010212.
[69] E. Giuliano, D. Paolino, M. C. Cristiano, M. Fresta, and D. Cosco, "Rutin-Loaded Poloxamer 407-Based Hydrogels for In Situ Administration: Stability Profiles and Rheological Properties," *Nanomaterials*, vol. 10, no. 6, Art. no. 6, Jun. 2020, doi: 10.3390/nano10061069.
[70] D. Monti *et al.*, "Poloxamer 407 microspheres for orotransmucosal drug delivery. Part II: In vitro/in vivo evaluation," *International Journal of Pharmaceutics*, vol. 400, no. 1, pp. 32–36, Nov. 2010, doi: 10.1016/j.ijpharm.2010.08.018.
[71] M. A. Abou-Shamat, J. Calvo-Castro, J. L. Stair, and M. T. Cook, "Modifying the Properties of Thermogelling Poloxamer 407 Solutions through Covalent Modification and the Use of Polymer Additives," *Macromolecular Chemistry and Physics*, vol. 220, no. 16, p. 1900173, 2019, doi: 10.1002/macp.201900173.
[72] N. Hirun, P. Kraisit, and V. Tantishaiyakul, "Thermosensitive Polymer Blend Composed of Poloxamer 407, Poloxamer 188 and Polycarbophil for the Use as Mucoadhesive In Situ Gel," *Polymers*, vol. 14, no. 9, Art. no. 9, Jan. 2022, doi: 10.3390/polym14091836.
[73] G. Li, Y. Lu, Y. Fan, Q. Ning, and W. Li, "Enhanced oral bioavailability of magnolol via mixed micelles and nanosuspensions based on Soluplus®-Poloxamer 188," *Drug Delivery*, vol. 27, no. 1, pp. 1010–1017, Jan. 2020, doi: 10.1080/10717544.2020.1785582.
[74] J. Chen *et al.*, "Effects of Commonly used Surfactants, Poloxamer 188 and Tween 80, on the Drug Transport Capacity of Intestinal Glucose Transporters," *AAPS PharmSciTech*, vol. 25, no. 6, p. 163, Jul. 2024, doi: 10.1208/s12249-024-02881-z.
[75] H. Gharib Khajeh, M. Sabzi, S. Ramezani, A. A. Jalili, and M. Ghorbani, "Fabrication of a wound dressing mat based on Polyurethane/Polyacrylic acid containing Poloxamer for skin tissue engineering," *Colloids and Surfaces A: Physicochemical and Engineering Aspects*, vol. 633, p. 127891, Jan. 2022, doi: 10.1016/j.colsurfa.2021.127891.
[76] J. Niyompanich, P. Chuysinuan, P. Pavasant, and P. Supaphol, "Development of thermoresponsive poloxamer in situ gel loaded with gentamicin sulfate for cavity wounds," *J Polym Res*, vol. 28, no. 4, p. 128, Mar. 2021, doi: 10.1007/s10965-020-02352-6.
[77] Y. Shang *et al.*, "Prospective application of poloxamer 188 in plastic surgery: A comprehensive review," *Chinese Journal of Plastic and*

*Reconstructive Surgery*, vol. 4, no. 1, pp. 31–37, Mar. 2022, doi: 10.1016/j.cjprs.2022.01.001.

[78] K. Mfoafo, Y. Kwon, Y. Omidi, and H. Omidian, "Contemporary applications of thermogelling PEO-PPO-PEO triblock copolymers," *Journal of Drug Delivery Science and Technology*, vol. 70, p. 103182, Apr. 2022, doi: 10.1016/j.jddst.2022.103182.

[79] M. M. Salzman, J. A. Bartos, D. Yannopoulos, and M. L. Riess, "Poloxamer 188 Protects Isolated Adult Mouse Cardiomyocytes from Reoxygenation Injury," *Pharmacology Research & Perspectives*, vol. 8, no. 6, p. e00639, 2020, doi: 10.1002/prp2.639.

[80] I. Babutan, O. Todor-Boer, L. I. Atanase, A. Vulpoi, S. Simon, and I. Botiz, "Self-assembly of block copolymers on surfaces exposed to space-confined solvent vapor annealing," *Polymer*, vol. 273, p. 125881, Apr. 2023, doi: 10.1016/j.polymer.2023.125881.

[81] I. Botiz, N. Grozev, H. Schlaad, and G. Reiter, "The influence of protic non-solvents present in the environment on structure formation of poly(γ-benzyl-L-glutamate) in organic solvents," *Soft Matter*, vol. 4, no. 5, pp. 993–1002, Apr. 2008, doi: 10.1039/B719946E.

[82] K. Jahanshahi *et al.*, "Crystallization of Poly(γ-benzyl l-glutamate) in Thin Film Solutions: Structure and Pattern Formation," *Macromolecules*, vol. 46, no. 4, pp. 1470–1476, Feb. 2013, doi: 10.1021/ma3024602.

[83] L. Li, R. Sun, and R. Zheng, "Tunable morphology and functionality of multicomponent self-assembly: A review," *Materials & Design*, vol. 197, p. 109209, Jan. 2021, doi: 10.1016/j.matdes.2020.109209.

[84] M. Stanisz, Ł. Klapiszewski, and T. Jesionowski, "Recent advances in the fabrication and application of biopolymer-based micro- and nanostructures: A comprehensive review," *Chemical Engineering Journal*, vol. 397, p. 125409, Oct. 2020, doi: 10.1016/j.cej.2020.125409.

[85] K. Ganguly, D. K. Patel, S. D. Dutta, W.-C. Shin, and K.-T. Lim, "Stimuli-responsive self-assembly of cellulose nanocrystals (CNCs): Structures, functions, and biomedical applications," *International Journal of Biological Macromolecules*, vol. 155, pp. 456–469, Jul. 2020, doi: 10.1016/j.ijbiomac.2020.03.171.

[86] A. Lupu, L. M. Gradinaru, V. R. Gradinaru, and M. Bercea, "Diversity of Bioinspired Hydrogels: From Structure to Applications," *Gels*, vol. 9, no. 5, Art. no. 5, May 2023, doi: 10.3390/gels9050376.

[87] "Effectiveness of bacteriophage JN01 incorporated in gelatin film with protocatechuic acid on biocontrol of Escherichia coli O157:H7 in beef - Li - 2022 - International Journal of Food Science & Technology - Wiley Online Library." Accessed: Aug. 08, 2024. [Online]. Available: https://ifst.onlinelibrary.wiley.com/doi/10.1111/ijfs.15673

[88] "Journal of Applied Polymer Science | Wiley Online Library." Accessed: Aug. 08, 2024. [Online]. Available: https://onlinelibrary.wiley.com/doi/10.1002/app.45351
[89] Y. Luo, Y. Wu, Y. Wang, and L. (Lucy) Yu, "Active and Robust Composite Films Based on Gelatin and Gallic Acid Integrated with Microfibrillated Cellulose," *Foods*, vol. 10, no. 11, Art. no. 11, Nov. 2021, doi: 10.3390/foods10112831.
[90] "Gels | Free Full-Text | Characterization of Tuna Gelatin-Based Hydrogels as a Matrix for Drug Delivery." Accessed: Aug. 08, 2024. [Online]. Available: https://www.mdpi.com/2310-2861/8/4/237
[91] S. Sinthusamran, S. Benjakul, Y. Hemar, and H. Kishimura, "Characteristics and Properties of Gelatin from Seabass (Lates calcarifer) Swim Bladder : Impact of Extraction Temperatures," *Waste Biomass Valor*, vol. 9, no. 2, pp. 315–325, Feb. 2018, doi: 10.1007/s12649-016-9817-5.
[92] X. Wu *et al.*, "Stability Enhanced Pickering Emulsions Based on Gelatin and Dialdehyde Starch Nanoparticles as Simple Strategy for Structuring Liquid Oils," *Food Bioprocess Technol*, vol. 14, no. 8, pp. 1600–1610, Aug. 2021, doi: 10.1007/s11947-021-02661-8.
[93] E. Jeevithan, R. Jeya Shakila, A. Varatharajakumar, G. Jeyasekaran, and D. Sukumar, "Physico-functional and mechanical properties of chitosan and calcium salts incorporated fish gelatin scaffolds," *International Journal of Biological Macromolecules*, vol. 60, pp. 262–267, Sep. 2013, doi: 10.1016/j.ijbiomac.2013.06.012.
[94] E. Yu *et al.*, "Gelatin from specific freshwater and saltwater fish extracted using six different methods: Component interactions, structural characteristics, and functional properties," *LWT*, vol. 191, p. 115656, Jan. 2024, doi: 10.1016/j.lwt.2023.115656.
[95] M. Wojcik, K. Kapusniak, A. Zarski, and J. Kapusniak, "Preparation and Characterization of Soluble Dextrin Fibre from Potato Starch Obtained on a Semi-Industrial Scale," *Applied Sciences*, vol. 14, no. 4, Art. no. 4, Jan. 2024, doi: 10.3390/app14041438.
[96] X. Chen *et al.*, "A Comparative Study of Resistant Dextrins and Resistant Maltodextrins from Different Tuber Crop Starches," *Polymers*, vol. 15, no. 23, Art. no. 23, Jan. 2023, doi: 10.3390/polym15234545.
[97] A. Beaussart, L. Parkinson, A. Mierczynska-Vasilev, and D. A. Beattie, "Adsorption of modified dextrins on molybdenite: AFM imaging, contact angle, and flotation studies," *Journal of Colloid and Interface Science*, vol. 368, no. 1, pp. 608–615, Feb. 2012, doi: 10.1016/j.jcis.2011.10.075.
[98] A. Mierczynska-Vasilev and D. A. Beattie, "In situ atomic force microscopy of modified dextrin adsorption on hydrophobic and hydrophilic layered silicate minerals," *Journal of Colloid and Interface*

*Science*, vol. 344, no. 2, pp. 429–437, Apr. 2010, doi: 10.1016/j.jcis.2010.01.009.

[99] D. A. Beattie, L. Huynh, A. Mierczynska-Vasilev, M. Myllynen, and J. Flatt, "Effect of Modified Dextrins on the Depression of Talc and Their Selectivity in Sulphide Mineral Flotation: Adsorption Isotherms, AFM Imaging and Flotation Studies," *Canadian Metallurgical Quarterly*, vol. 46, no. 3, pp. 349–358, Sep. 2007, doi: 10.1179/cmq.2007.46.3.349.

[100] Q. A. Besford *et al.*, "Protein Component of Oyster Glycogen Nanoparticles: An Anchor Point for Functionalization," *ACS Appl. Mater. Interfaces*, vol. 12, no. 35, pp. 38976–38988, Sep. 2020, doi: 10.1021/acsami.0c10699.

[101] M. Pais, S. D. George, and P. Rao, "Glycogen nanoparticles as a potential corrosion inhibitor," *International Journal of Biological Macromolecules*, vol. 182, pp. 2117–2129, Jul. 2021, doi: 10.1016/j.ijbiomac.2021.05.185.

[102] J.-H. Ryu *et al.*, "Comparative structural analyses of purified glycogen particles from rat liver, human skeletal muscle and commercial preparations," *International Journal of Biological Macromolecules*, vol. 45, no. 5, pp. 478–482, Dec. 2009, doi: 10.1016/j.ijbiomac.2009.08.006.

[103] M. A. Sullivan, F. Vilaplana, R. A. Cave, D. Stapleton, A. A. Gray-Weale, and R. G. Gilbert, "Nature of $\alpha$ and $\beta$ Particles in Glycogen Using Molecular Size Distributions," *Biomacromolecules*, vol. 11, no. 4, pp. 1094–1100, Apr. 2010, doi: 10.1021/bm100074p.

[104] P. Zhang, S. S. Nada, X. Tan, B. Deng, M. A. Sullivan, and R. G. Gilbert, "Exploring glycogen biosynthesis through Monte Carlo simulation," *International Journal of Biological Macromolecules*, vol. 116, pp. 264–271, Sep. 2018, doi: 10.1016/j.ijbiomac.2018.05.027.

[105] K. Nagpal, S. K. Singh, and D. N. Mishra, "Chitosan Nanoparticles: A Promising System in Novel Drug Delivery," *Chemical and Pharmaceutical Bulletin*, vol. 58, no. 11, pp. 1423–1430, 2010, doi: 10.1248/cpb.58.1423.

[106] K. Divya and M. S. Jisha, "Chitosan nanoparticles preparation and applications," *Environ Chem Lett*, vol. 16, no. 1, pp. 101–112, Mar. 2018, doi: 10.1007/s10311-017-0670-y.

[107] D. J. Sullivan, M. Cruz-Romero, T. Collins, E. Cummins, J. P. Kerry, and M. A. Morris, "Synthesis of monodisperse chitosan nanoparticles," *Food Hydrocolloids*, vol. 83, pp. 355–364, Oct. 2018, doi: 10.1016/j.foodhyd.2018.05.010.

[108] M. Li and M. Xin, "N,N-Dilauryl chitosan self-assembled vesicles for drug delivery," *Designed Monomers and Polymers*, vol. 9, no. 1, pp. 89–97, Jan. 2006, doi: 10.1163/156855506775526179.

[109] Q. Li, E. T. Dunn, E. W. Grandmaison, and M. F. A. Goosen, "Applications and Properties of Chitosan," in *Applications of Chitan and Chitosan*, CRC Press, 1996.
[110] V. K. Mourya and N. N. Inamdar, "Chitosan-modifications and applications: Opportunities galore," *Reactive and Functional Polymers*, vol. 68, no. 6, pp. 1013–1051, Jun. 2008, doi: 10.1016/j.reactfunctpolym.2008.03.002.
[111] H. Y. Zhang, E. Arab Tehrany, C. J. F. Kahn, M. Ponçot, M. Linder, and F. Cleymand, "Effects of nanoliposomes based on soya, rapeseed and fish lecithins on chitosan thin films designed for tissue engineering," *Carbohydrate Polymers*, vol. 88, no. 2, pp. 618–627, Apr. 2012, doi: 10.1016/j.carbpol.2012.01.007.
[112] A. Sionkowska and A. Płanecka, "Surface properties of thin films based on the mixtures of chitosan and silk fibroin," *Journal of Molecular Liquids*, vol. 186, pp. 157–162, Oct. 2013, doi: 10.1016/j.molliq.2013.07.008.
[113] H. Jiang, W. Su, S. Caracci, T. J. Bunning, T. Cooper, and W. W. Adams, "Optical waveguiding and morphology of chitosan thin films," *Journal of Applied Polymer Science*, vol. 61, no. 7, pp. 1163–1171, 1996, doi: 10.1002/(SICI)1097-4628(19960815)61:7<1163::AID-APP12>3.0.CO;2-Z.
[114] L. Balau, G. Lisa, M. Popa, V. Tura, and V. Melnig, "Physico-chemical properties of Chitosan films," *Open Chemistry*, vol. 2, no. 4, pp. 638–647, Dec. 2004, doi: 10.2478/BF02482727.
[115] W. F. Yap, W. M. M. Yunus, Z. A. Talib, and N. A. Yusof, "X-ray photoelectron spectroscopy and atomic force microscopy studies on crosslinked chitosan thin film," *Int. J. Phys. Sci.*.
[116] W. H. Nosal, D. W. Thompson, L. Yan, S. Sarkar, A. Subramanian, and J. A. Woollam, "UV–vis–infrared optical and AFM study of spin-cast chitosan films," *Colloids and Surfaces B: Biointerfaces*, vol. 43, no. 3, pp. 131–137, Jul. 2005, doi: 10.1016/j.colsurfb.2004.08.022.
[117] W. H. Nosal, D. W. Thompson, L. Yan, S. Sarkar, A. Subramanian, and J. A. Woollam, "Infrared optical properties and AFM of spin-cast chitosan films chemically modified with 1,2 Epoxy-3-phenoxy-propane," *Colloids and Surfaces B: Biointerfaces*, vol. 46, no. 1, pp. 26–31, Nov. 2005, doi: 10.1016/j.colsurfb.2005.08.006.
[118] S. Tan *et al.*, "Adsorption of chitosan onto carbonaceous surfaces and its application: atomic force microscopy study," *Nanotechnology*, vol. 22, no. 15, p. 155703, Mar. 2011, doi: 10.1088/0957-4484/22/15/155703.
[119] R. Chandrasekaran, R. P. Millane, S. Arnott, and E. D. T. Atkins, "The crystal structure of gellan," *Carbohydrate Research*, vol. 175, no. 1, pp. 1–15, Apr. 1988, doi: 10.1016/0008-6215(88)80151-4.

[120] T. Funami *et al.*, "Molecular Structures of Gellan Gum Imaged with Atomic Force Microscopy in Relation to the Rheological Behavior in Aqueous Systems in the Presence or Absence of Various Cations," *J. Agric. Food Chem.*, vol. 56, no. 18, pp. 8609–8618, Sep. 2008, doi: 10.1021/jf8007713.
[121] "Biosubstrates Obtained from Gellan Gum for Organic Light-Emitting Diodes | ACS Applied Electronic Materials." Accessed: Aug. 08, 2024. [Online]. Available: https://pubs.acs.org/doi/10.1021/acsaelm.1c00217
[122] "Effects of Partial Replacement of Gelatin in High Sugar Gels with Gellan on their Textural, Rhelogical, and Thermal Properties | Food Biophysics." Accessed: Aug. 08, 2024. [Online]. Available: https://link.springer.com/article/10.1007/s11483-016-9454-3
[123] L. Severini *et al.*, "Methacrylated gellan gum hydrogel: a smart tool to face complex problems in the cleaning of paper materials," *Cellulose*, vol. 30, no. 16, pp. 10469–10485, Nov. 2023, doi: 10.1007/s10570-023-05479-z.
[124] P. Zhang, A. Tang, B. Zhu, L. Zhu, and H. Zeng, "Hierarchical Self-Assembly of Dopamine into Patterned Structures," *Advanced Materials Interfaces*, vol. 4, no. 11, p. 1601218, 2017, doi: 10.1002/admi.201601218.
[125] "Surface Characteristics of a Self-Polymerized Dopamine Coating Deposited on Hydrophobic Polymer Films | Langmuir." Accessed: Aug. 09, 2024. [Online]. Available: https://pubs.acs.org/doi/10.1021/la202877k
[126] "Characterization of Polydopamine Thin Films Deposited at Short Times by Autoxidation of Dopamine | Langmuir." Accessed: Aug. 09, 2024. [Online]. Available: https://pubs.acs.org/doi/10.1021/la400587j
[127] G. Fricke, R. Carpenter, and R. Battino, "Effect of Various Gases on the pH of Water," *J. Phys. Chem.*, vol. 77, no. 6, pp. 826–827, Mar. 1973, doi: 10.1021/j100625a600.
[128] I. J. Beyerlein, M. J. Demkowicz, A. Misra, and B. P. Uberuaga, "Defect-interface interactions," *Progress in Materials Science*, vol. 74, pp. 125–210, Oct. 2015, doi: 10.1016/j.pmatsci.2015.02.001.
[129] P. Lejček, M. Šob, and V. Paidar, "Interfacial segregation and grain boundary embrittlement: An overview and critical assessment of experimental data and calculated results," *Progress in Materials Science*, vol. 87, pp. 83–139, Jun. 2017, doi: 10.1016/j.pmatsci.2016.11.001.
[130] G. Gyulai and E. Kiss, "Interaction of poly(lactic- co -glycolic acid) nanoparticles at fluid interfaces," *Journal of Colloid and Interface Science*, vol. 500, pp. 9–19, Aug. 2017, doi: 10.1016/j.jcis.2017.03.114.
[131] D. Ramya, P. Sandhya, and Dr. B. V. Hari, "Poloxamer: A Novel Functional Molecule For Drug Delivery And Gene Therapy," *Journal of Pharmaceutical Sciences and Research*, vol. 5. Jul. 07, 2013.

[132] E. Giuliano, D. Paolino, M. Fresta, and D. Cosco, "Mucosal Applications of Poloxamer 407-Based Hydrogels: An Overview," *Pharmaceutics*, vol. 10, no. 3, p. 159, Sep. 2018, doi: 10.3390/pharmaceutics10030159.
[133] K. Burts, T. Plisko, A. Bildyukevich, A. Penkova, and S. Pratsenko, "Modification of polysulfone ultrafiltration membranes using block copolymer Pluronic F127," *Polymer Bulletin*, vol. 78, pp. 1–28, Nov. 2021, doi: 10.1007/s00289-020-03437-4.
[134] E. Guzniczak, M. Jimenez, M. Irwin, O. Otto, N. Willoughby, and H. Bridle, "Impact of poloxamer 188 (Pluronic F-68) additive on cell mechanical properties, quantification by real-time deformability cytometry," *Biomicrofluidics*, vol. 12, no. 4, p. 044118, Aug. 2018, doi: 10.1063/1.5040316.
[135] J. Li, B. Munjal, C. Zeng, and R. Suryanarayanan, "Dual Functionality of Poloxamer 188 in Freeze-Dried Protein Formulations: A Stabilizer in Frozen Solutions and a Bulking Agent in Lyophiles," *Mol. Pharmaceutics*, vol. 21, no. 5, pp. 2555–2564, May 2024, doi: 10.1021/acs.molpharmaceut.4c00108.
[136] R. A. Patel, "A MORPHOLOGICAL STUDY OF NANOMATERIALS AND BIOMOLECULES USING ATOMIC FORCE MICROSCOPY".
[137] S. Kotova, V. Timofeeva, G. Belkova, N. Aksenova, and A. Solovieva, "Porphyrin effect on the surface morphology of amphiphilic polymers as observed by atomic force microscopy," *Micron (Oxford, England : 1993)*, vol. 43, pp. 445–9, Nov. 2011, doi: 10.1016/j.micron.2011.10.025.
[138] G. Wu and K. Y. C. Lee, "Effects of Poloxamer 188 on Phospholipid Monolayer Morphology: An Atomic Force Microscopy Study," *Langmuir*, vol. 25, no. 4, pp. 2133–2139, Feb. 2009, doi: 10.1021/la802908x.